

# Robust Immersive Bilateral Teleoperation of Dissimilar Systems with Enhanced Transparency and Sense of Embodiment

Mahdi Hejrati , Pauli Mustalahti , and Jouni Mattila 

**Abstract**—In human-in-the-loop systems such as teleoperation, especially those involving heavy-duty manipulators, achieving high task performance requires both robust control and strong human engagement. This paper presents a bilateral teleoperation framework that enhances the operator’s Sense of Embodiment (SoE)—specifically, the senses of agency and self-location—through an immersive virtual reality interface and distributed haptic feedback via an exoskeleton. To support this embodiment and establish high level of motion and force transparency, we develop a force-sensorless, robust control architecture that tackles input nonlinearities, master-slave asymmetries, unknown uncertainties, and arbitrary time delays. A human–robot augmented dynamic model is integrated into the control loop to enhance human-adaptability of the controller. Theoretical analysis confirms semi-global uniform ultimate boundedness of the closed-loop system. Extensive real-world experiments demonstrate high accuracy tracking under up to 1:13 motion scaling and 1:1000 force scaling, showcasing the significance of the results. Additionally, the stability-transparency tradeoff for motion tracking and force reflection-tracking is established up to 150 ms of one-way fix and time-varying communication delay. The results of user study with 10 participants (9 male and 1 female) demonstrated that the system can imply a good level of SoE (76.4%), at the same time is very user friendly with no gender limitation. These results are significant given the scale and weight of the heavy-duty manipulators.

**Index Terms**—Bilateral teleoperation control, time delay, transparency, virtual reality, haptic display.

## I. INTRODUCTION

**T**ELEOPERATED robotic systems, first introduced by Goertz in the 1940s [1], integrate human cognitive abilities with control-theoretic approaches to enable remote operation of robots in environments that are hazardous, unstructured, or otherwise unsuitable for direct human presence. In scenarios where fully autonomous systems remain impractical or unsafe, teleoperation offers a robust and flexible alternative, with proven effectiveness across a wide range of domains [2]–[4]. One domain with significant untapped potential for teleoperation is heavy-duty robotic operation, particularly through the use of heavy-duty hydraulic manipulators (HHMs). These machines are already widely deployed in industries such as mining, construction, and forestry, where they handle physically intensive tasks in dynamic and often dangerous environments. Through teleoperation, HHMs can be leveraged not only to extend human capabilities into these heavy-duty contexts but also to enable remote skill transfer from human

This work is supported by Business Finland partnership project “Future all-electric rough terrain autonomous mobile manipulators” (Grant 2334/31/222). Corresponding author: Mahdi Hejrati

All authors are with the Department of Engineering and Natural Science, Tampere University, 7320 Tampere, Finland (e-mail: mahdi.hejrati@tuni.fi, jouni.mattila@tuni.fi, pauli.mustalahti@tuni.fi).

operators to machines [5], addressing a key bottleneck in the automation of HHMs [6].

Despite the advantages of teleoperation, task performance often deteriorates during remote operation due to factors such as master-slave mismatches, communication delays, and non-intuitive human-machine interfaces that can cause cyber sicknesses [7]. These challenges become even more pronounced when teleoperating HHMs, whose scale, dynamics, and mechanical complexity make them significantly less tractable than lightweight robotic systems. These issues disrupt the operator’s natural sensorimotor loop and can impair proprioceptive perception, causing the control to feel indirect or disjointed. One effective approach to mitigate these effects is enhancing the operator’s sense of *presence* [8], defined as the subjective experience of being physically situated at the remote site, which, in the context of teleoperation, is more precisely referred to as the sense of *telepresence* (SoT) [9], [10]. Nonetheless, enhancing telepresence alone is not sufficient to ensure high-quality task execution in teleoperation by a human operator.

Slater (2009) [11] argued that Place Illusion—his proposed refinement of the term “presence”—is not sufficient on its own for users to behave realistically in virtual environments. He introduced the concept of Plausibility Illusion (Psi), defined as the illusion that events occurring in the virtual environment are actually happening. According to Slater, both Place Illusion and Plausibility Illusion must co-occur for users to generate realistic responses within the virtual context. Building on this framework, Kilteni et al. (2012) [12] emphasized that realistic actions in virtual environments are closely linked to the sense of embodiment (SoE). Within the concept of teleoperation, SoE is defined as a psychological state in which the operator experiences the remote robotic system as an extension of their own body. According to [12], [13], SoE encompasses three critical components: (1) *body ownership*—feeling the remote robot as part of oneself; (2) *self-location*—a strong spatial presence at the remote site; and (3) *agency*—the confidence that one’s intentions directly produce corresponding actions in the remote environment. In many real-world applications—particularly industrial and field scenarios—the most relevant embodiment components are agency and self-location [13], which directly influence the operator’s control quality and task performance.

Thus, a strong SoE is crucial for successful teleoperation. When the SoE is strong, the operator no longer perceives the surrogate, the teleoperated robot, as an external tool, but rather as an extension of their own body and sensorimotor system [14]. This shift minimizes cognitive load and enhances the fluidity of task execution. Immersion is one key to evoking

this sense of embodiment. Through the combination of visual feedback, delivered via a VR headset, and distributed haptic feedback from force-reflective exoskeletons, immersive bilateral teleoperation creates more realistic task operation. But for immersion to truly support embodiment, it must be grounded in two essential pillars, each addressing relevant components of SoE: precise control, which reinforces the operator's sense of agency, and appropriate equipment, which anchors their sense of self-location.

This study addresses both dimensions in the context of industrial surrogates, focusing on heavy-duty hydraulic manipulators (HHMs). By developing a robust, high-accuracy control framework and pairing it with immersive, well-integrated hardware, we aim to strengthen both agency and self-location. This enables HHMs to combine human-like precision with mechanical strength, empowering operators to perform complex tasks efficiently and safely in hazardous or unstructured environments.

## II. RELATED WORKS

### A. Sense of Self-Location

Immersive bilateral teleoperation relies on the integration of multi-modal sensory feedback, including visual, auditory, and haptic cues, to foster a stronger connection between the human operator and the remote environment. This immersive experience enhances the SoT, which in turn reinforces the Sense of Self-Location, as the two are closely interlinked. It is important to note, however, that not all sensory inputs contribute equally to immersion. Visual feedback, in particular, plays a foundational role in shaping the immersive experience during teleoperation [15]. Yet, immersion itself is a qualitative and often comparative concept [11]; one system can be considered as more immersive than another with the given visual feedback, if, for instance, it provides real-time egocentric head-tracking compared to one with static camera. Even within the same system configuration, enhancements such as higher display resolution or the addition of haptic feedback can further elevate the sense of immersion, and, by extension, strengthen the operator's sense of self-location.

Building upon this foundation, Cheng et al. [16] introduce Open-TeleVision, an immersive teleoperation system that allows operators to intuitively perceive the robot's environment in a stereoscopic manner. Central to their approach is a stereo RGB camera mounted on the humanoid robot's head, equipped with a 2-DoF actuation mechanism that dynamically tracks the operator's head movements. This configuration enables real-time, egocentric visual feedback streamed directly to a VR device, effectively strengthening the operator's sense of being present in the remote environment. Transitioning from single-view perception to a more comprehensive spatial awareness, [17] proposes a system for dual-arm bilateral teleoperation that further boosts the sense of embodiment. Their method combines multi-view visual feedback with haptic interaction, offering the operator five distinct visual sections—each from different camera perspectives—alongside real-time force graphs and parameter reconfiguration. This multi-faceted feedback setup allows the operator to maintain a heightened situational

awareness, contributing to more precise and confident task execution. The immersive teleoperation framework proposed in [18] increased the task execution performance by balancing the trade-off between data streaming costs and data visual quality in immersive VR. Other papers, moreover, leveraged the enhanced VR to achieve higher degrees of immersion in teleoperation [19], [20]. Expanding on the integration of sensory modalities, [21] presents a visual-haptic perception and reconstruction system designed to enhance telepresence. Their system not only delivers visual information from the remote site through VR but also provides haptic guidance to the operator, fostering a stronger cognitive and physical connection to the task environment.

Collectively, these works highlight a consistent theme: the sense of presence, mostly driven by synchronized visual feedback, is pivotal for effective and high-performance teleoperation. As recent research continues to demonstrate, the more immersive and responsive the feedback, the stronger the operator's sense of self-location becomes, ultimately enabling more intuitive and accurate teleoperation.

### B. Sense of Agency

As the sense of agency heavily rely on the trust of operator on that his/her actions will be mirrored by the remote robot, amplifying this sense requires design of adaptive and robust control algorithm for reliable bilateral teleoperation control. From the perspective of control theory, accomplishment of such an objective relies on two criteria: *stability* and *transparency* [1] of the bilateral teleoperation system. The primary stability issue in bilateral teleoperation arises from time delays in the communication medium between the master and slave robots [22]. In addition, stability can be adversely affected by the system's interaction with both the human (active) and the environment (passive). Meanwhile, low transparency often stems from unknown uncertainties in the human/master and the slave/environment models. Though they may appear to be distinct objectives, stability and transparency are deeply interconnected. The central challenge in this field lies in achieving a high level of both, without compromising either [23]. Over the past few decades, extensive research has been conducted to address these objectives [24], [25]. Therefore, enhancing the sense of agency fundamentally depends on achieving stable and transparent bilateral teleoperation control. This necessitates the development of robust and high-performance control strategies that can guarantee reliable and intuitive operation.

Many advanced control methods have been developed for electric master-slave systems with similar configurations [26]–[29], where joint-to-joint mapping is employed to close the control loop, limiting the applicability of methods to slave robots with dissimilar configurations. Dissimilar lightweight systems with differing configurations and workspaces have also been investigated in the literature [30]–[33]. For example, in [34], a Force Dimension Sigma 7 haptic device is employed to teleoperate a 7-DoF KUKA robots by designing passivity-based admittance control scheme in the presence of time delay. The dissimilarity, furthermore, in the sense of cooperative

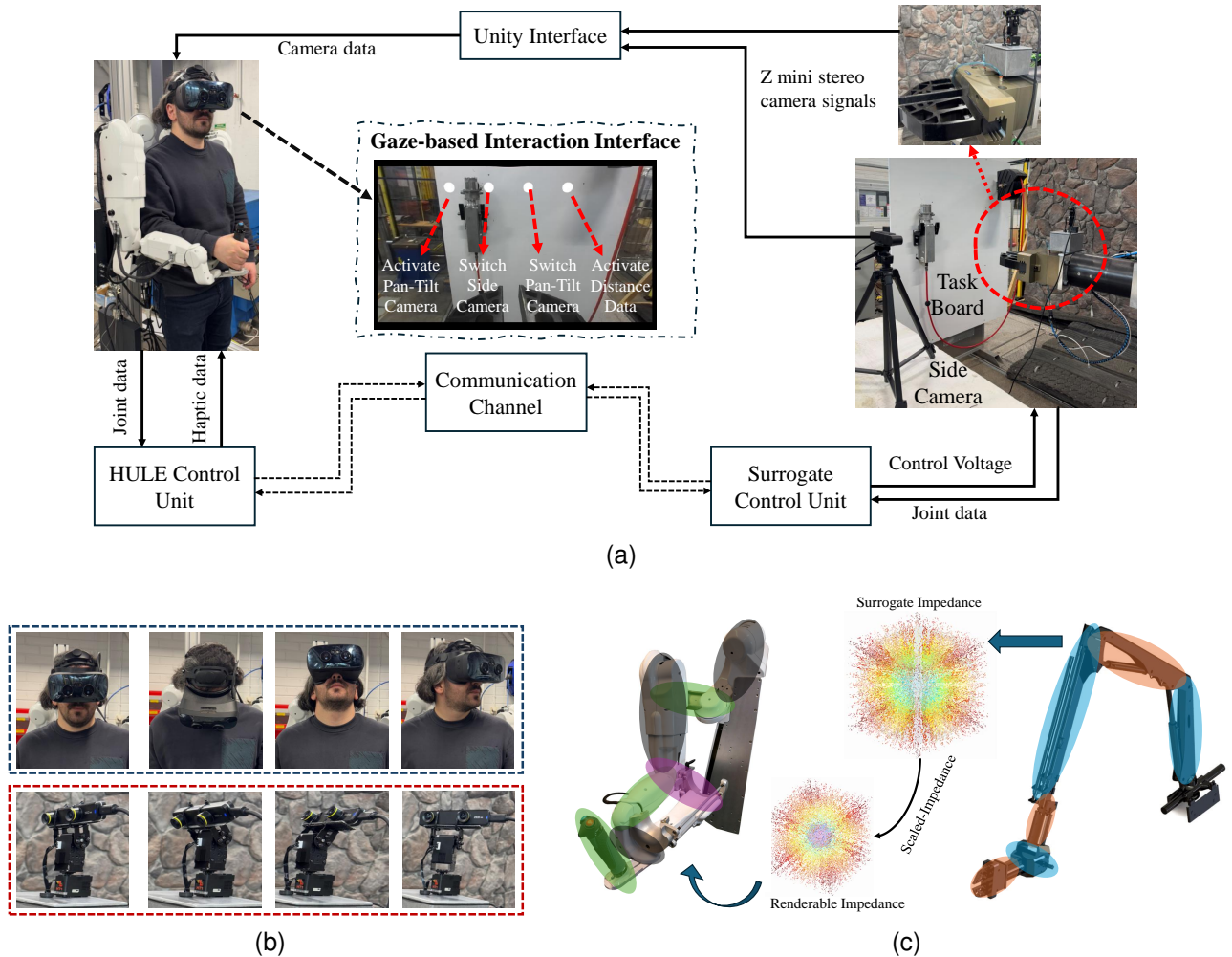


Fig. 1. Scheme of the VR-based immersive bilateral teleoperation system with egocentric head tracking. (a) Overview of the general teleoperation framework, featuring control units, communication channels, and a gaze-based interaction interface. By utilizing the eye-tracking capability of the VR headset, the interface enables the operator to switch between modes based on gaze direction. The side, also, camera enhances situational awareness, especially in cases where the operator encounters difficulties during manipulation. (b) Pan-tilt mechanism of the remote camera, synchronized with the human operator's egocentric head movements to maintain intuitive visual feedback. (c) Visualization of the rendered and distributed scaled impedance of the remote robot onto the human operator's arm. The utilized HULE enables the operator to perceive both the dynamics of the remote robot and its interactions with the remote environment.

teleoperation with single master and multi or bimanual slave systems has also been widely examined [35], [36]. However, research on bilateral teleoperation of hydraulically actuated manipulators remains limited due to the governing fluid dynamics and highly nonlinear characteristics of such actuators. Most studies rely on linear control theory [37] or 1-DoF slave systems [38], [39], which may not be suitable for controlling nonlinear and complex systems in real-world applications.

With increased attention to controlling hydraulically driven actuators using advanced control schemes and addressing accuracy and stability challenges, studies such as [40]–[43] have paved the way for achieving stable and high-fidelity bilateral teleoperation of hydraulic manipulators. In [44], [45], the bilateral teleoperation of 2-DoF HHMs with arbitrary motion-force scaling is examined, incorporating estimated human exogenous force and slave/environment interaction forces to ensure stability and transparency. Furthermore, [46] investigates the bilateral teleoperation of 2-DoF HHMs in contact with both physical and virtual environments. To overcome the poor

dynamics of HHMs, an integration of locally weighted intent prediction with a blended shared control method is proposed in [47]. The operational inefficiency of asymmetric master-slave hydraulic manipulators is addressed in [48] through a novel human-machine interface that enhances vision and incorporates auditory feedback.

Consequently, the focus of the literature on bilateral teleoperation control primarily revolves around symmetric 1 : 1 scale systems, dissimilar systems with low DoF in master/slave robots, or cases where the orientation of the slave robot is largely ignored, with a predominant concentration on lightweight electric robots. However, teleoperation of large, heavy robots requires more attention than their electric counterparts due to the unique challenges of their automation and control, such as high scaling of force/motion. Such a drawback can degrade the operator trust to control algorithm, reducing the teleoperation task performance. Therefore, there is a crucial need for robust and high-performance control algorithm to address all the challenges of the hydraulically-actuated

robotic manipulators, yet establish a good level transparency and stability for the immersive bilateral teleoperation setup.

### C. Aims and Contributions

Building on the previous discussion, this paper aims to significantly improve the accuracy and performance of bilateral teleoperation for large, heavy-duty robotic systems by enhancing immersion and reinforcing the operator's SoE. As depicted in Fig. 1a, we integrate a head-tracked pan-tilt camera system mounted on the surrogate robot, which synchronizes in real time with the operator's natural egocentric head movements. This two-DoF visual setup, as shown in Fig. 1b, delivers immersive, first-person feedback that aligns with the operator's viewpoint, reinforcing spatial presence and self-location [15]. Complementing the visual feedback, we employ the ABLE system, a 7-DoF HULE [49], to deliver rich proprioceptive input (Fig. 1c). This device distributes the equivalent impedance of the remote manipulator along the operator's arm while reflecting contact forces, further strengthening the physical and cognitive link between operator and surrogate. The combination of high-fidelity visual and proprioceptive cues significantly elevates the operator's sense of presence and self-location, both critical to effective teleoperation. In parallel, we design a robust, high-accuracy control framework capable of stabilizing the complex human-in-the-loop teleoperation system under model uncertainties, time delays, and external disturbances. By maintaining stable and responsive behavior, this control architecture strengthens the operator's Sense of Agency, fostering trust, precision, and control throughout the task. Therefore, the unique contributions of this work can be summarized as follows:

- A VR-based visual feedback system with egocentric head-tracking is employed to deliver immersive, perspective-aligned visuals. The integrated VR headset also includes eye-tracking, enabling gaze-contingent resolution enhancement, a feature known to further heighten visual immersion. To deepen the embodied experience, a wearable haptic exoskeleton provides both contact force reflection and the distributed impedance of the remote manipulator. Together, these technologies substantially reinforce the SoE during task execution.
- A novel control strategy is developed to ensure the stability and transparency of the force-reflective bilateral teleoperation system. It accounts for the human-robot augmented dynamics, unknown model parameters, and arbitrary time delays. By embedding an interaction force estimation module for both the human/master and slave/environment sides, the proposed controller is well-suited for real-world deployment on heavy-duty manipulators, enabling intuitive, stable operation while enhancing the operator's Sense of Agency.
- The proposed framework is deployed on a real-world heavy-duty teleoperation setup. Extensive experiments are conducted to evaluate the system's robustness, transparency, and accuracy in both free-motion and contact-rich scenarios. Additionally, user studies assess the system's usability and its effectiveness in enhancing SoE during task performance.

Beyond improving task performance in challenging heavy-duty scenarios, the proposed system also serves as a rich platform for data collection and skill transfer. Its immersive, embodied setup is ideally suited for training learning-based models, including imitation learning, an area gaining traction particularly in the context of lightweight and humanoid systems [16], [50]. This work thus lays a foundational step toward the full automation of heavy-duty robotic systems, combining human expertise with machine capability in a scalable, data-driven manner.

The rest of the paper is organized as follows. Section II explains the mathematical preliminaries. Section III and IV elaborate on control design and stability analysis of master and slave robots, respectively. Section V is dedicated to stability and transparency analysis of force-reflective bilateral teleoperation setup. The experimental results are provided in Section VI. Finally, Section VI concludes this study.

## III. MATHEMATICAL PRELIMINARIES

In this section, the mathematical foundation of the controller is explained along with the lemmas and assumptions employed in the rest of the paper.

### A. Virtual Decomposition Control

Virtual decomposition control (VDC) scheme is based on Plucker coordinate with compact formulation of system dynamics based on 6-D Plucker basis. In this coordinate system,  $\mathcal{M}^6$  denotes the space of spatial motions, while  $\mathcal{F}^6$  represents the space of spatial forces. Within these coordinates and spaces for a given frame  $\{A\}$  attached to the body of a rigid body, the spatial velocity and force vectors can be defined as,

$${}^A V = [{}^A v, {}^A \omega]^T \in \mathcal{M}^6, \quad {}^A F = [{}^A f, {}^A \tau]^T \in \mathcal{F}^6$$

with  ${}^A v$ ,  ${}^A \omega$ ,  ${}^A f$ ,  ${}^A \tau$  being linear velocity, angular velocity, linear force, and moment with respect to frame  $\{A\}$ . The spatial forces and velocity vectors can be transformed between frames as,

$${}^B V = {}^B U_A^T {}^A V, \quad {}^B F = {}^B U_A {}^A F \quad (1)$$

with  ${}^B U_A$  being transformation matrix between two frames.

VDC scheme decomposes the system into rigid body and joint parts for each of which the modeling, control, and stability analysis are performed separately. Then local stability is extended to the stability of entire system by means of virtual power flow (VPF). Within this context, the dynamics of the rigid body is independent of the system and is expressed in 6-D vector as,

$$M_A \frac{d}{dt} ({}^A V) + C_A ({}^A \omega) {}^A V + G_A(t) = {}^A F^* \quad (2)$$

with  $M_A \in \mathbb{R}^{6 \times 6}$ ,  $C_A \in \mathbb{R}^{6 \times 6}$ , and  $G_A \in \mathbb{R}^6$  being spatial mass, centrifugal, gravitational matrices with  ${}^A F^* \in \mathbb{R}^6$  being net spatial force applied to the rigid body, all defined in Plucker coordinates.

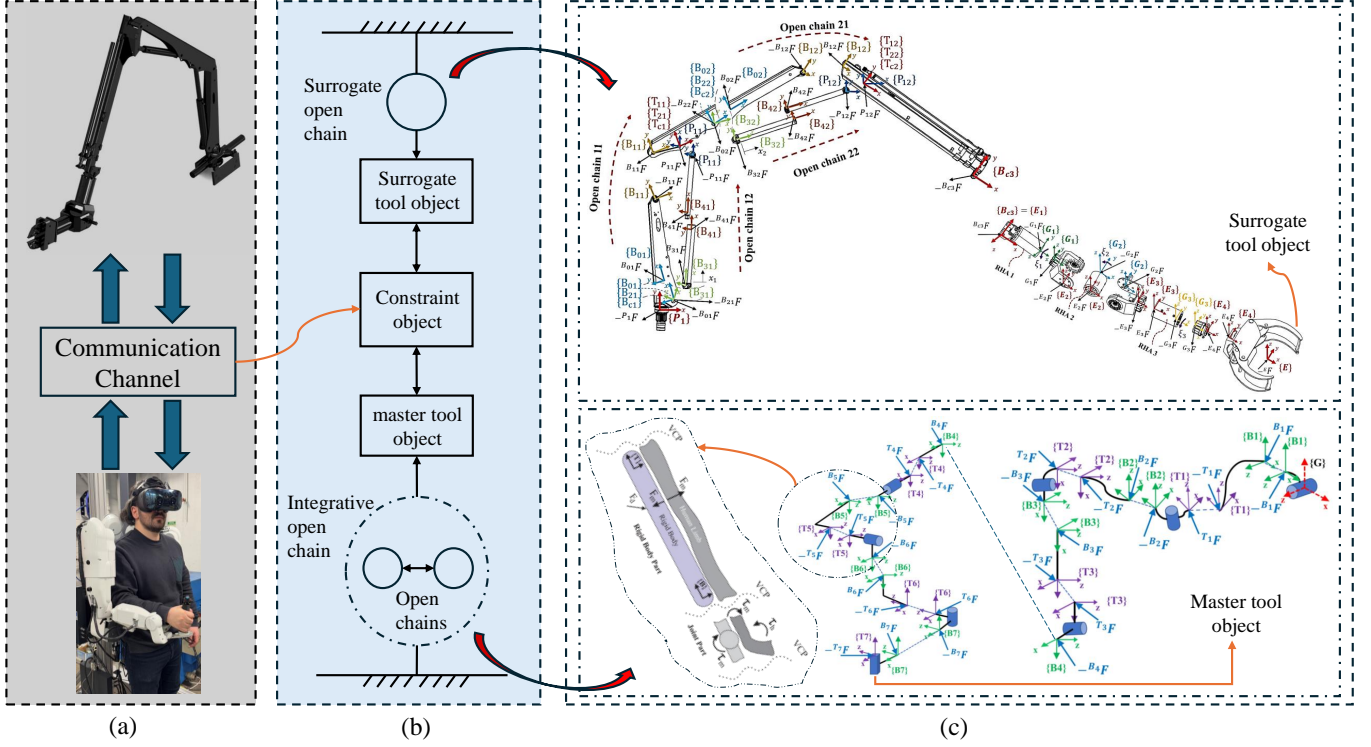


Fig. 2. Proposed control method for robust and transparent force-reflected bilateral teleoperation. (a) Schematic of an immersive bilateral teleoperation system. (b) Graph-based representation of the proposed teleoperation control strategy. Open chains represent serial robotic manipulators; the "object" denotes the connective constraint linking two open chains; and the integrative open chain models the interconnected structure of the exoskeleton's serial links and the human arm. (c) Virtual decomposition of the master and surrogate systems. The integrative open chain highlights how the augmented human–robot model is seamlessly incorporated into the control framework. Details regarding the decomposition of the master robot and surrogate system can be found in [51] and [52], respectively.

*Property 1:* [53] The rigid body dynamics in (2) can be written in linear-in-parameter form as,

$$M_A \frac{d}{dt}({}^A V) + C_A({}^A \omega) {}^A V + G_A(t) = \bar{Y}_A({}^A \dot{V}, {}^A V) \phi_A$$

with  $\bar{Y}_A({}^A \dot{V}, {}^A V) \in \mathbb{R}^{6 \times 10}$  being regression matrix and  $\phi_A(m_A, h_A, I_A) \in \mathbb{R}^{10}$  being known inertial parameter vector. Additionally,  $m_A$ ,  $h_A$ , and  $I_A$  are mass, first mass moment, and rotational inertia matrix, respectively.

*Definition 1:* For the given frame  $\{A\}$ , the VPF is defined as the inner product of the spatial velocity vector error and the spatial force vector error, that is,

$$p_A = ({}^A \mathcal{V}_r - {}^A \mathcal{V})^T ({}^A F_r - {}^A F)$$

*Definition 2:* A non-negative accompanying function  $\nu(t) \in \mathbb{R}$  is a piecewise, differentiable function defined  $\forall t \in \mathbb{R}^+$  with  $\nu(0) < \infty$  and  $\dot{\nu}(t)$  exists almost everywhere.

*Lemma 1:* [52] Consider a complex robot that is virtually decomposed into subsystems. Each subsystem is said to be virtually semi-globally uniformly ultimately bounded with its non-negative accompanying function  $\nu(t)$  and its affiliated vector  $\dot{\nu}(t)$ , if and only if,

$$\dot{\nu} \leq -\alpha_1 \nu + \alpha_{10} + p_A - p_C \quad (3)$$

with  $\alpha_1$  and  $\alpha_{10}$  being positive constants and  $p_A$  and  $p_C$  denoting the sum of VPFs in the sense of Definition 1.

Since VDC is a velocity-based controller, the role of the required joint velocity is critical, as its proper definition enables the assignment of different tasks to the controller. By appropriately defining the required angular velocity, one can achieve free motion, in-contact motion, or hybrid motion/force control. In this study, as the goal is to design a controller for dissimilar bilateral teleoperation, the required end-effector velocity is first defined as in (13) and (37). Using the Jacobian matrix, the corresponding required joint velocity is then computed as shown in (14) and (38).

### B. Lemmas and Definitions

*Lemma 2:* Thanks to their universal approximation capability, radial basis function neural networks (RBFNNs) can be employed to estimate any given continuous function  $f(t)$  represented in frame  $\{A\}$  as,

$$\hat{f}_A(t) = {}^A \hat{W}^T \psi(\chi_A) + {}^A \epsilon$$

with  $\chi_A$  being the input vector,  $\hat{W}$  being the estimated weights,  $\psi(\cdot)$  being Gaussian basis function, and  $\epsilon$  being estimation error of the RBFNNs. The adaptation laws for estimation of weights and bias of the network can be considered as follows [52],

$$\begin{aligned} \dot{{}^A \hat{W}} &= \Pi \left( \psi(\chi_A) ({}^A V_r - {}^A V)^T - \tau_0 {}^A \hat{W} \right) \\ \dot{{}^A \epsilon} &= \pi (({}^A V_r - {}^A V) - \pi_0 {}^A \epsilon), \end{aligned}$$

where  $\Pi, \tau_0, \pi, \pi_0$  are positive constants. Under the optimal weights of RBFNNs as,

$$W^* = \arg \min_{\hat{W} \in \Xi_N} \{ \sup_{\chi \in \Xi_T} |\hat{\mathbf{f}}(\chi|\hat{W}) - \mathbf{f}(\chi)| \}$$

where  $\Xi_N = \{\hat{W} \mid \|\hat{W}\| \leq \kappa\}$  is a valid set of vectors with  $\kappa$  being a design value,  $\Xi_T$  is an allowable set of the state vectors, there is,

$$|\hat{\mathbf{f}}(\chi) - {}^A W^{*T} \psi(\chi_A)| = |\epsilon^*(\chi_A)| \leq \bar{\epsilon} \quad (4)$$

where  $\bar{\epsilon}$  is an unknown bound parameters.

*Lemma 3:* [54] Let  $k_b > 0$  be a positive constant, and define the sets  $\mathfrak{Z} := \{\mathfrak{z} \in \mathbb{R} : -k_b < \mathfrak{z} < k_b\} \subset \mathbb{R}$  and  $\mathcal{N} := \mathbb{R}^l \times \mathfrak{Z} \subset \mathbb{R}^{l+1}$ , which are open. Consider the dynamical system:

$$\dot{\eta} = \hbar(t, \eta),$$

where  $\eta := [\omega, \mathfrak{z}]^\top \in \mathcal{N}$ , and  $\hbar : \mathbb{R}_+ \times \mathcal{N} \rightarrow \mathbb{R}^{l+1}$  is piecewise continuous in  $t$  and locally Lipschitz in  $\eta$ , uniformly in  $t$ , on  $\mathbb{R}_+ \times \mathcal{N}$ . Suppose there exist functions  $\mathfrak{U} : \mathbb{R}^l \rightarrow \mathbb{R}_+$  and  $\mathfrak{V} : \mathfrak{Z} \rightarrow \mathbb{R}_+$ , both continuously differentiable and positive definite in their respective domains, such that:

$$\begin{aligned} \mathfrak{V}(\mathfrak{z}) &\rightarrow \infty \quad \text{as} \quad \mathfrak{z} \rightarrow -k_b \quad \text{or} \quad \mathfrak{z} \rightarrow k_b, \\ \delta_7(\|\omega\|) &\leq \mathfrak{U}(\omega) \leq \delta_8(\|\omega\|), \end{aligned}$$

where  $\delta_7$  and  $\delta_8$  are class  $\mathcal{K}_\infty$  functions. Let  $V(\eta) := \mathfrak{V}(\mathfrak{z}) + \mathfrak{U}(\omega)$ , and assume  $\mathfrak{z}(0) \in (-k_b, k_b)$ . If the following inequality holds:

$$\dot{V} = \frac{\partial V}{\partial \eta} \hbar \leq 0,$$

then  $\mathfrak{z}(t)$  remains in the open set  $(-k_b, k_b)$  for all  $t \in [0, \infty)$ .

*Definition 3:* For any unique representation of inertial parameter vector of rigid body  $\phi_A$ , there is one-to-one map as,

$$\mathcal{N}(\phi_A) = \mathcal{L}_A = \begin{bmatrix} 0.5tr(\bar{I}) \cdot \mathbf{1} - I & h \\ h^T & m \end{bmatrix}$$

$$\mathcal{N}^{-1}(\mathcal{L}_A) = \phi_A(m, h, tr(\Sigma) \cdot \mathbf{1} - \Sigma)$$

where  $\Sigma = 0.5tr(I) - I$  and  $tr(\cdot)$  is the Trace operator of a matrix.

*Definition 4:* For a given  $\mathcal{L}_A$  with its estimation  $\hat{\mathcal{L}}_A$ , the natural adaptation law (NAL) can be derived as,

$$\dot{\hat{\mathcal{L}}}_A = \frac{1}{\gamma} \hat{\mathcal{L}}_A \left( \mathcal{S}_A - \gamma_0 \hat{\mathcal{L}}_A \right) \hat{\mathcal{L}}_A \quad (5)$$

with  $\gamma > 0$  being the adaptation gain for all the rigid bodies of the system, and  $\gamma_0 > 0$  being a small positive gain. Additionally,  $\mathcal{S}_A$  is a unique symmetric matrix defined in [51].

### C. Notation

In the remainder of the paper the following notation are used. For a given signal  $\mathbf{n}$ , the filtered signal  $\mathbf{\hat{n}}$  is computed as:

$$\dot{\mathbf{n}} + \mathcal{C} \mathbf{n} = \mathcal{C} \mathbf{n},$$

where  $\mathcal{C}$  is a positive constant for scalar signals and positive-definite matrix for vectors. The  $\hat{\mathbf{n}}$  represents the estimation of  $\mathbf{n}$  while  $\tilde{\mathbf{n}} = \hat{\mathbf{n}} - \mathbf{n}$ . The  ${}^A \mathbf{n}$  represents the signal defined in frame  $\{A\}$ .

### IV. AUGMENTED HUMAN/MASTER DYNAMICS AND CONTROL

The master robot utilized in this study is a 7-DoF HULE, which serves as both an exoskeleton and a haptic display, depicted in Fig. 3. The details of the controller design are presented below. The decentralized human-robot augmented model proposed by [51] can be written as follows,

$$\mathcal{M}_B \frac{d}{dt} ({}^{B_i} \mathcal{V}) + \mathcal{C}_{B_i} {}^{B_i} \mathcal{V} + \mathcal{G}_{B_i} = {}^{B_i} \mathcal{F}^* - \Delta_{D_i} \quad (6)$$

$$\mathcal{I}_i \ddot{q}_i = \tau_i^* - \tau_{h_i} - \Delta_i \quad (7)$$

$$\tau_i = \tau_i^* + \tau_{a_i} \quad (8)$$

where  $\mathcal{M}_B = M_r + M_h \in \mathbb{R}^{6 \times 6}$ ,  $\mathcal{C}_B = C_r + C_h \in \mathbb{R}^{6 \times 6}$ , and  $\mathcal{G}_B = G_r + G_h \in \mathbb{R}^{6 \times 6}$  are augmented matrices in the form of (2),  $\mathcal{I} = I_r + I_h \in \mathbb{R}^6$  being augmented rotational inertia of the joint with  $(.)_r$  standing for robot and  $(.)_h$  representing human-related terms,  $\tau_h$  being exogenous human torque (EHT),  $\Delta_D \in \mathbb{R}^6$  and  $\Delta_J \in \mathbb{R}^6$  encompassing unmodeled dynamics and compound input nonlinearity for rigid body and joint subsystems, respectively.

*Remark 1:* Equation (8) presents the recomposed dynamics of the decomposed system. The first term on the right-hand side of (8) represents the torque responsible for generating joint-level actions, while the second term,  $\tau_a = \sigma^T {}^B \mathcal{F}$  where  ${}^B \mathcal{F}$  defined in (11), corresponds to the forces arising from the motion of the rigid body. It worth to note that the screw vector  $\sigma$  maps the spatial force  ${}^B \mathcal{F}$  from space spatial forces space to the joint space.

Being grounded in the Newton-Euler recursive method, VDC necessitates the computation of forward spatial velocity and acceleration, as well as backward spatial force propagation. These steps are fundamental for designing the control law in Plücker coordinates. In the following, the computation process is detailed for the 7-DoF HULE.

1) *Kinematics and Dynamics:* Considering the framing convention depicted in Fig. 3a, the spatial velocity vectors for the  $i$ -th link of the decentralized system can be derived starting from the base frame as follows:

$${}^{B_i} \mathcal{V} = {}^{T_{i-1}} U_{B_i}^T {}^{T_{i-1}} \mathcal{V} + \sigma_i \dot{q}_i, \quad (9)$$

$${}^{T_i} \mathcal{V} = {}^{B_i} U_{T_i}^T {}^{B_i} \mathcal{V}, \quad (10)$$

for  $i = 1, \dots, 7$ . Once the spatial velocity and, consequently, the spatial acceleration are computed, the spatial forces can be determined as follows:

$${}^{B_j} \mathcal{F} = {}^{B_j} U_{T_j} {}^{T_j} \mathcal{F} + {}^{B_j} \mathcal{F}^*, \quad (11)$$

$${}^{T_{j-1}} \mathcal{F} = {}^{T_{j-1}} U_{B_j} {}^{B_j} \mathcal{F}, \quad (12)$$

for  $j = 7, \dots, 1$ , where  ${}^{B_j} \mathcal{F}^*$  represents the net spatial force applied to frame  $\{B\}$  as defined in (6). Fig. 3b illustrates the frames and spatial forces applied to the  $i^{th}$  decomposed subsystem. With the dynamics defined in (6)–(12), the corresponding control action can now be designed, as explained in the following sections.

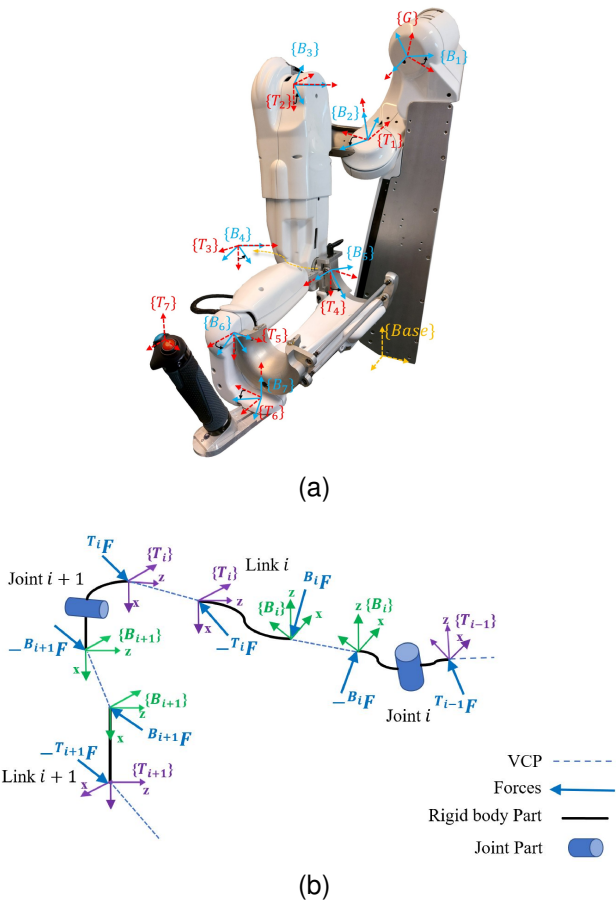


Fig. 3. Decomposition of HULE using the VCP concept. a) Framing convention in VDC context, b)  $i^{th}$  subsystem of decomposed model

2) *Control design:* Considering the bilateral teleoperation task with either free motion or in-contact operation, the required end-effector velocity of master robot can be defined as,

$$V_{mr} = V_{md} - \mathcal{A}F_m. \quad (13)$$

with  $V_{md} \in \mathbb{R}^6$  expressed in (54). Then, using the pseudo-inverse of the HULE Jacobian  $\mathcal{J}_m \in \mathbb{R}^{6 \times 7}$ , the joint level required velocity can be derived as,

$$\dot{q}_r = \mathcal{J}_m^\dagger V_{mr}. \quad (14)$$

The velocity term in (14) represents the motion that must be generated by the actuators of the master robot to fulfill the objectives of teleoperation. With this notion, the required spatial velocity of the rigid bodies can be computed by substituting (14) into (9)–(10) as follows:

$${}^{B_i}\mathcal{V}_r = {}^{T_{i-1}}U_{B_i}^T {}^{T_{i-1}}\mathcal{V}_r + \sigma_i \dot{q}_r \quad (15)$$

$${}^{T_i}\mathcal{V}_r = {}^{B_i}U_{T_i}^T {}^{B_i}\mathcal{V}_r. \quad (16)$$

In the context of VDC, the forces that generate the required spatial velocities are referred to as required spatial forces. These forces correspond to those that would produce the required velocity described in (15) if applied to the rigid body. Consequently, the required spatial forces can be expressed as follows:

$${}^{B_j}\mathcal{F}_r = {}^{B_j}U_{T_j} {}^{T_j}\mathcal{F}_r + {}^{B_j}\mathcal{F}_r^* \quad (17)$$

$${}^{T_{j-1}}\mathcal{F}_r = {}^{T_{j-1}}U_{B_j} {}^{B_j}\mathcal{F}_r. \quad (18)$$

with  ${}^{B_j}\mathcal{F}_r^*$  being the required net spatial force of the rigid body defined in (20). Finally, the unified required joint torque can be computed in the sense of (8) as,

$$\tau_{ri} = \tau_{ri}^* + \tau_{ari} \quad (19)$$

with  $\tau_{ari} = \sigma_i^T {}^{B_i}\mathcal{F}_r$ , and  $\tau_{ri}^*$  defined in (21). Addressing the unknown uncertainties and dynamics of the rigid bodies and joints, the control signal in (19) achieves the objectives of the teleoperation system by generating the required joint velocity described in (14).

*Lemma 4:*

*Theorem 1:* For the decentralized and augmented model of pHRI described in (6)–(8), along with the spatial velocity and force computations in (9)–(12) and (15)–(18), the decentralized control actions can be designed as follows:

$${}^{B_i}\mathcal{F}_r^* = \mathcal{K}_{Di}({}^{B_i}\mathcal{V}_r - {}^{B_i}\mathcal{V}) + \hat{W}_{Di}^T \Psi(\chi_{Di}) + \hat{\varepsilon}_{Di} + Y_{B_i} \hat{\phi}_{B_i} \quad (20)$$

$$\begin{aligned} \tau_{ri}^* = k_{di}(\dot{q}_{ri} - \dot{q}_i) + Y_{ai} \hat{\phi}_{ai} + \hat{W}_{Ji}^T \Psi(\chi_{Ji}) \\ + \hat{\varepsilon}_{Ji} + \frac{e_{ai} + c_1 \dot{e}^T e_{ai}^2}{k_{bi}^2 - e_{ai}^2} \end{aligned} \quad (21)$$

which ensures the SGUUB of all signals in the closed loop system. Additionally, the followings hold,

$$e_{ai} \in \Omega_e, \quad (22)$$

$$\rho_m \stackrel{\text{def}}{=} V_{mr} - V_m = V_{md} - V_m - \mathcal{A}F_m \in \Omega_m, \quad (23)$$

$$\Omega_m \stackrel{\text{def}}{=} \{V_{mr} - V_m \in \mathbb{R}^6 \mid \|V_{mr} - V_m\| \leq \mathcal{D}_m\} \quad (24)$$

$$\Omega_e \stackrel{\text{def}}{=} \{e_{ai} \in \mathbb{R} \mid |q_{ri} - q_i| \leq \mathcal{D}_1, \|\dot{q}_{ri} - \dot{q}_i\| \leq \mathcal{D}_2\}. \quad (25)$$

*Proof 1:* Defining non-negative accompanying function as,

$$\nu_m(t) = \sum_{i=1}^7 (\nu_i(t) + \nu_{ai}(t)) \quad (26)$$

$$\begin{aligned} \nu_i(t) = \frac{1}{2}({}^{B_i}\mathcal{V}_r - {}^{B_i}\mathcal{V})^T \mathcal{M}_{B_i}({}^{B_i}\mathcal{V}_r - {}^{B_i}\mathcal{V}) \\ + \gamma_1 \mathcal{D}_F(\mathcal{L}_{B_i} \|\hat{\mathcal{L}}_{B_i}) + \frac{1}{2} \text{tr}(\tilde{W}_{Di}^T \Gamma_{B_i}^{-1} \tilde{W}_{Di}) \\ + \frac{1}{2\gamma_{2i}} \tilde{\varepsilon}_{Di}^T \tilde{\varepsilon}_{Di}. \end{aligned} \quad (27)$$

$$\begin{aligned} \nu_{ai}(t) = \frac{1}{2} \mathcal{I}_i(\dot{q}_{ri} - \dot{q}_i)^2 + \frac{1}{2} \log \frac{k_{bi}^2}{k_{bi}^2 - e_{ai}^2} \\ + \zeta \mathcal{D}_F(\mathcal{L}_{ai} \|\hat{\mathcal{L}}_{ai}) + \frac{1}{2\beta_{2i}} \tilde{\varepsilon}_{Ji}^2 + \frac{1}{2\beta_{1i}} \tilde{W}_{Ji}^T \tilde{W}_{Ji} \end{aligned} \quad (28)$$

and taking its time derivative, replacing adaptation functions from Lemma 2 and (5), the local controllers in (20) and (21) along with employing Young's inequality as  $-\text{tr}(\hat{\mathcal{L}}_{B_i} \tilde{\mathcal{L}}_{B_i}) \leq -0.5\text{tr}(\hat{\mathcal{L}}_{B_i} \tilde{\mathcal{L}}_{B_i}) + 0.5\text{tr}(\mathcal{L}_{B_i} \mathcal{L}_{B_i})$ ,  $-\text{tr}(\tilde{W}_{Di}^T \tilde{W}_{Di}) \leq -0.5\text{tr}(\tilde{W}_{Di}^T \tilde{W}_{Di}) + 0.5\text{tr}(W_{Di}^T W_{Di})$ ,

$-\tilde{\varepsilon}_{Di}^T \tilde{\varepsilon}_{Di} \leq -0.5 \tilde{\varepsilon}_{Di}^T \tilde{\varepsilon}_{Di} + 0.5 \varepsilon_{Di}^T \varepsilon_{Di}$ ,  $-\tilde{\varepsilon}_{Ji}^T \tilde{\varepsilon}_{Ji} \leq -0.5 \tilde{\varepsilon}_{Ji}^T \tilde{\varepsilon}_{Ji} + 0.5 \varepsilon_{Ji}^T \varepsilon_{Ji}$ , we have,

$$\begin{aligned} \dot{\nu}_m(t) &\leq -\sum_{i=1}^n [(\mathcal{B}_i \mathcal{V}_r - \mathcal{B}_i \mathcal{V})^T \mathcal{K}_{Di} (\mathcal{B}_i \mathcal{V}_r - \mathcal{B}_i \mathcal{V}) \\ &\quad + k_{di}(\dot{q}_{ri} - \dot{q}_i)^2 + 0.5\gamma_{0m} \text{tr}(\tilde{\mathcal{L}}_{B_i} \tilde{\mathcal{L}}_{B_i}) \\ &\quad + 0.5\tau_{0m} \text{tr}(\tilde{W}_{Di}^T \tilde{W}_{Di}) + \pi_{0m} \tilde{\varepsilon}_{Di}^T \tilde{\varepsilon}_{Di} + \pi_{0m} \tilde{\varepsilon}_{Ji}^T \tilde{\varepsilon}_{Ji} \\ &\quad + 0.5\gamma_{0m} \text{tr}(\tilde{\mathcal{L}}_{ai} \tilde{\mathcal{L}}_{ai}) + 0.5\tau_{0m} \text{tr}(\tilde{W}_{Ji}^T \tilde{W}_{Ji}) \\ &\quad + c_1 \frac{e_{ai}^2}{k_{bi}^2 - e_{ai}^2}] + \sum_{i=1}^n [0.5\gamma_{0m} \text{tr}(\mathcal{L}_{B_i} \mathcal{L}_{B_i}) \\ &\quad + 0.5\tau_{0m} \text{tr}(W_{Di}^T W_{Di}) + \pi_{0m} \varepsilon_{Di}^T \varepsilon_{Di} + \pi_{0m} \varepsilon_{Ji}^T \varepsilon_{Ji} \\ &\quad + 0.5\gamma_{0m} \text{tr}(\mathcal{L}_{ai} \mathcal{L}_{ai}) + 0.5\tau_{0m} \text{tr}(W_{Ji}^T W_{Ji})] \\ &\leq -\vartheta \nu_m(t) + \vartheta_0 - p_{T_7} \end{aligned} \quad (29)$$

where  $\vartheta_0 = 0.5\gamma_{0m} \text{tr}(\mathcal{L}_{B_i} \mathcal{L}_{B_i}) + 0.5\tau_{0m} \text{tr}(W_{Di}^T W_{Di}) + \pi_{0m} \varepsilon_{Di}^T \varepsilon_{Di} + \pi_{0m} \varepsilon_{Ji}^T \varepsilon_{Ji} + 0.5\gamma_{0m} \text{tr}(\mathcal{L}_{ai} \mathcal{L}_{ai}) + 0.5\tau_{0m} \text{tr}(W_{Ji}^T W_{Ji})$ , and  $\vartheta = \vartheta_{min}/\vartheta_{max}$ , with  $\vartheta_{min} = \min(\min(k_{di}), \min(\mathcal{K}_{Di}), \gamma_{0m}, \tau_{0m}, c_1, \pi_{0m})$  and,

$$\begin{aligned} \vartheta_{max} &= \max(\max(M_{B_i}), \max(\mathcal{K}_{Di}), \gamma_{1m}, \max(\Gamma_{B_i}), \\ &\quad \max(\gamma_{2i}^{-1}), \max(\mathcal{L}_i), \max(\beta_{2i}^{-1}), \max(\beta_{1i}^{-1}), \zeta, 1), \end{aligned} \quad (30)$$

where the following inequality is used,

$$\log \frac{k_{bi}^2}{k_{bi}^2 - e_{ai}^2} \leq \frac{e_{ai}^2}{k_{bi}^2 - e_{ai}^2}. \quad (31)$$

According to (29) all the VPFs cancel out each other as shown in Appendix B of [51] except  $p_{T_7}$ , which indicates the virtual power flow between human hand and the robot. Then, by integrating both side of (29), one can obtain,

$$\nu_m(t) \leq \nu(0) e^{-\vartheta t} + \frac{\vartheta_0}{\vartheta} (1 - e^{-\vartheta t}) + \varrho_m. \quad (32)$$

with  $\varrho_m$  defined in Appendix A. According to (32) and Appendix A, the maximum and steady-state value of  $\nu_m$  can be derived as,  $\nu_m(t) \leq \nu_{max} = \nu(0) + \vartheta_0/\vartheta + \varrho_m$  and  $\lim_{t \rightarrow \infty} \nu_m(t) \leq \vartheta_0/\vartheta + \varrho_{0m}$ , with  $\varrho_{0m}$  defined in Appendix A. Then, the following holds from (26),

$$\frac{1}{2} \log \frac{k_{bi}^2}{k_{bi}^2 - e_{ai}^2} \leq \nu_m(t) \leq \nu_{max}. \quad (33)$$

Taking the exponential on both sides of (33) and rearranging the terms, we can show that,

$$|e_{ai}| \leq k_{bi} \sqrt{1 - e^{-2\nu_{max}}} = \mathcal{D}_1. \quad (34)$$

In the same way, it can be shown that,

$$\|\dot{q}_{ri} - \dot{q}_i\| \leq \sqrt{\frac{2\nu_{max}}{\lambda_{min}(\mathcal{L}_i)}} = \mathcal{D}_2 \quad (35)$$

$$\|V_{mr} - V_m\| \leq \alpha_m \sqrt{\frac{2\nu_{max}}{\lambda_{min}(M_{B_7})}} = \mathcal{D}_m. \quad (36)$$

with  $\|B^7 U_{T_7}\| \leq \alpha_m$ . Additionally, considering Lemma 3 and (32), we have  $|e_{ai}| \leq k_{bi}$ . Then from  $q_i = q_{ri} - e_{ai}$  and  $|q_{ri}| \leq k_{ri}$ , we can conclude that  $|q_i| \leq k_{ci} = k_{ri} + k_{bi}$  if  $e_{ai}(0) \leq k_{bi}$ , ensuring that state-constraints will not be violated.

## V. SLAVE/ENVIRONMENT DYNAMICS AND CONTROL

The slave robot in this study is a 6-DoF HHM with a 3-DoF anthropomorphic arm and a spherical wrist, shown in Fig. 4, encompassing the complexities arising from fluid dynamics and the nonlinearities of a high-DoF system. The primary objective of the slave robot is to accurately follow the motion and force commands from the master robot while ensuring stable contact with an unknown environment. Furthermore, since the use of force sensors in HHMs is not always a feasible solution, a force-sensorless control law is designed to address this issue effectively.

For doing so, the required end-effector velocity of the slave robot can be defined as,

$$V_{sr} = V_{sd} - \mathcal{A} \hat{\mathbf{F}}_s \quad (37)$$

with  $V_{sd}$  defined in (55). Then, using the damped least square (DLS) inverse of Jacobian matrix  $\mathcal{J}_s \in \mathcal{R}^{6 \times 6}$ , one can obtain the required joint velocity as follows,

$$\dot{\theta}_r = \{(\mathcal{J}_s^T \mathcal{J}_s + \lambda I)^{-1} \mathcal{J}_s^T\} V_{sr} \quad (38)$$

with  $\lambda \in \mathcal{R}$  being damping factor. The use of the Damped Least Squares (DLS) method tackles the gimbal lock effect, which is a common phenomenon in spherical wrists. To enhance readability and avoid redundancy, only the tool of the slave robot is considered to demonstrate the control design in this study. The comprehensive analysis of the entire system, for both free-motion and in-contact tasks, is elaborated upon in [52], [55]. Therefore, as shown in Fig. 4, it is assumed that the velocity computations and force backpropagations are performed up to frame  $\{G_3\}$  for both  $\dot{\theta}$  and  $\dot{\theta}_r$  in (38), as described in [52].

At the time of contact, the following hold

$${}^T F = N_c f_e \quad (39)$$

where,

$$f_e = M_e \dot{V}_s + D_e V_s + K_e \mathbf{x}_e \quad (40)$$

with  $\mathbf{x}_e$  being the deformation of the environment,  $M_e$ ,  $D_e$ , and  $K_e$  being the environmental mass, damping, and stiffness matrices, respectively, all of which are unknown. Therefore, the force resultant on the tool body can be written,

$${}^{G_3} F^* = {}^{G_3} F - {}^{G_3} U_T {}^T F, \quad (41)$$

where, the net spatial force vector  ${}^{G_3} F^*$  of the tool can be written in the sense of (2) as,

$$M_{G_3} \frac{d}{dt} ({}^{G_3} V) + C_{G_3} ({}^{G_3} \omega) {}^{G_3} V + G_{G_3} + {}^{G_3} \Delta_R(t) = {}^{G_3} F^*. \quad (42)$$

with  $\Delta_R(t)$  being unknown uncertainty. Considering (38), the following hold,

$${}^{G_3} V_r = {}^T U_{G_3}^T {}^T V_r, \quad (43)$$

$${}^T F_r = N_c f_{ed}, \quad (44)$$

$${}^{G_3} F_r^* = Y_{G_3} \hat{\phi}_{G_3} + K_{G_3} ({}^{G_3} V_r - {}^{G_3} V) + {}^{G_3} \hat{\Delta}_R, \quad (45)$$

$$f_{ed} = M_e \dot{V}_{sr} + D_e V_s + K_e \mathbf{x}_e. \quad (46)$$

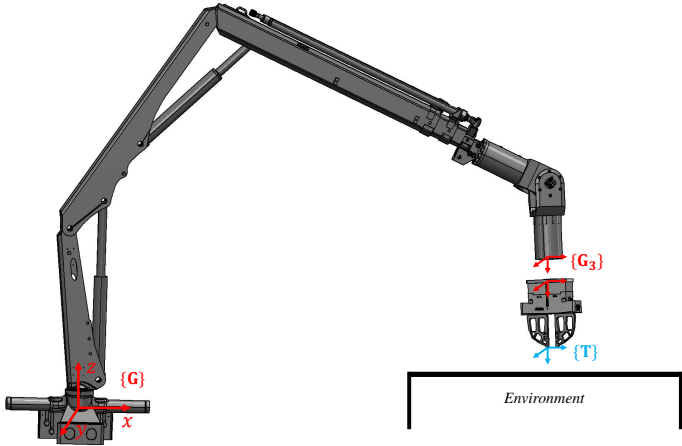


Fig. 4. Scheme of 6-DoF HHM in presence of unknown environment

where  ${}^{G_3}\hat{\Delta}_R$  is in the sense of Lemma 2. According to (41), the required spatial force vector, which acts as the control signal for tool body, can be written as,

$${}^{G_3}F_r = {}^{G_3}F_r^* + {}^{G_3}U_T^T F_r. \quad (47)$$

Consequently, the required piston force can be computed as,

$$f_{cr} = \frac{1}{r_w} \sigma^T {}^{G_3}F_r + \sigma^T {}^{G_{p3}}F_r^* \quad (48)$$

where  $r_w$  being gear ratio of helical gears in the actuator and  ${}^{G_{p3}}F_r^*$  being the net required spatial force of piston body in the sense of (45).

*Remark 2:* The first term in (48) accounts for the dynamics of the rigid body subsystem, while the second term compensates for the joint mechanism's dynamics and uncertainties, ensuring the fulfillment of the control objectives. The low-level voltage control for generating the required piston force follows the approach outlined in [52].

*Theorem 2:* The tool of the slave manipulator with dynamics represented in (42) and required net spatial force defined in (45) is virtually SGUUB.

*Proof 2:* Following the same procedure in Theorem 2 of [55] for frame  $\{G_3\}$  with non-negative accompanying function  $\nu_{G_3}$ , the following holds,

$$\dot{\nu}_{G_3} \leq -\mu \nu_{G_3} + \mu_0 + p_{G_3} - p_T \quad (49)$$

with  $\mu$  and  $\mu_0$  being positive constants,  $p_{G_3}$  being VPF of driving cutting point, and  $p_T$  is the VPF between slave robot end-effector and environment. According to Lemma 1 and (49), the tool subsystem is virtually SGUUB.

*Lemma 5:* The following holds for  $p_T$ ,

$$\lim_{t \rightarrow \infty} \int_0^t p_T dt \geq -\varrho_{0s} \quad (50)$$

where  $\varrho_{0s}$  is a positive constant.

*Proof 3:* Appendix B.

*Theorem 3:* Consider the slave robot decomposed into subsystems employing VCP concept. Then, for all  $\mathbf{A} \in \Psi$ ,

where  $\Psi$  encompasses all the rigid body frames attached to the subsystem except  $\{G_3\}$ , with,

$$\nu_s = \nu_{G_3} + \sum_{\mathbf{A} \in S} \nu_{\mathbf{A}} + \sum_{j=1,6} (f_{pj} - f_{pj})^2 / (2\beta k_{xj}). \quad (51)$$

all the signals of the closed-loop system are SGUUB. Consequently, the following holds,

$$\rho_s \stackrel{\text{def}}{=} V_{sr} - V_s = V_{sd} - V_s - \mathcal{A}F_s \in \Omega_s. \quad (52)$$

where

$$\Omega_s \stackrel{\text{def}}{=} \{V_{sr} - V_s \in \mathbb{R}^6 \mid \|V_{sr} - V_s\| \leq \alpha \sqrt{\frac{2(\bar{\mu}_0 + \varrho_s)}{\lambda_{\min}(M_{G_3})\bar{\mu}}}\}. \quad (53)$$

where  $\|{}^{G_3}U_T^T\| \leq \alpha_s$ ,  $\|p_T\| \geq \varrho_s$  with  $\bar{\mu}$  and  $\bar{\mu}_0$  being positive constants.

*Proof 4:* The proof follows the same approach as outlined in Theorem 3 of [52] and Theorem 1, using Lemma (5).

## VI. DISSIMILAR BILATERAL TELEOPERATION

In this section, the desired master and slave velocities, denoted as  $V_{md} \in \mathcal{R}^6$  and  $V_{sd} \in \mathcal{R}^6$ , are designed to enable dissimilar bilateral teleoperation through the communication channel with motion/force scaling. To achieve this, we define:

$$V_{md} = \kappa_p^{-1} (\mathbf{V}_s + \Lambda [\mathbf{X}_s - \kappa_p \mathbf{X}_m] - \mathcal{A} [\mathbf{F}_s + (\kappa_f - \kappa_p) \mathbf{F}_m]), \quad (54)$$

$$V_{sd} = \kappa_p (\mathbf{V}_m + \Lambda \mathbf{X}_m) - \Lambda \mathbf{X}_s - \mathcal{A} \kappa_f \mathbf{F}_m, \quad (55)$$

where  $\kappa_p \in \mathcal{R}^{6 \times 6}$  and  $\kappa_f \in \mathcal{R}^{6 \times 6}$  are the motion and force scaling matrices, respectively;  $\Lambda \in \mathcal{R}^{6 \times 6}$  is a positive-definite matrix; and  $\mathbf{X}_m$ ,  $\mathbf{V}_m$ ,  $\mathbf{X}_s$ , and  $\mathbf{V}_s$  represent the pose and velocity of the master robot and the pose and velocity of the slave robot end-effectors, respectively.

### A. Stability Analysis

1) *Stability without delay:* Substituting (54) and (55) into (23) and (52), respectively, with  $\dot{\mathbf{X}}_m = \mathbf{V}_m$  and  $\dot{\mathbf{X}}_s = \mathbf{V}_s$ , we can write,

$$\begin{aligned} \rho_s - \kappa_p \rho_m &= \kappa_p \mathbf{V}_m - \mathbf{V}_s + \Lambda [\kappa_p \mathbf{X}_m - \mathbf{X}_s] + \kappa_p \mathbf{V}_m \\ &\quad - \mathbf{V}_s + \Lambda [\kappa_p \mathbf{X}_m - \mathbf{X}_s] \\ &= \mathbf{e} + \mathbf{e} \end{aligned} \quad (56)$$

with,

$$\mathbf{e} \stackrel{\text{def}}{=} \kappa_p \mathbf{V}_m - \mathbf{V}_s + \Lambda [\kappa_p \mathbf{X}_m - \mathbf{X}_s]. \quad (57)$$

According to results of Theorem 1 and 3 along with (56), one can obtain,

$$\mathbf{e} \in \Omega_T \quad (58)$$

$$\Omega_T \stackrel{\text{def}}{=} \{\mathbf{e} \in \mathbb{R}^6 \mid \|\mathbf{e}\| \leq \alpha_s \sqrt{\frac{2(\bar{\mu}_0 + \varrho_s)}{\lambda_{\min}(M_{G_3})\bar{\mu}}} + \kappa_p \mathcal{D}_m\} \quad (59)$$

leading to,

$$\rho_v \stackrel{\text{def}}{=} \kappa_p \mathbf{V}_m - \mathbf{V}_s \in \Omega_T \quad (60)$$

$$\rho_p \stackrel{\text{def}}{=} \kappa_p X_m - X_s \in \Omega_T. \quad (61)$$

The above equations ensure the boundedness of velocity and position errors during both free-motion and in-contact operations in the presence of unknown uncertainties, human exogenous forces, and environmental contacts.

2) *Stability with delay*: In order to address time delays existing in communication medium between master and slave robot, the expressions in (54) and (55) can be modified as,

$$V_{md} = \kappa_p^{-1} (e^{-s\mathcal{T}} (\mathbf{V}_s + \Lambda \mathbf{X}_s) - \kappa_p \Lambda X_m - \mathcal{A} [e^{-s\mathcal{T}} \mathbf{F}_s + (\kappa_f - \kappa_p) \mathbf{F}_m]) \quad (62)$$

$$V_{sd} = e^{-s\mathcal{T}} \kappa_p (\mathbf{V}_m + \Lambda \mathbf{X}_m) - \Lambda X_s - e^{-s\mathcal{T}} \mathcal{A} \kappa_f \mathbf{F}_m \quad (63)$$

with  $\mathcal{T}$  being one-way arbitrary time delay. Substituting (62) and (63) in (23) and (52), one can obtain,

$$\kappa_p (\mathbf{V}_m + \Lambda \mathbf{X}_m) + \mathcal{A} \kappa_f \mathbf{F}_m = e^{-s\mathcal{T}} [\mathbf{V}_s + \Lambda \mathbf{X}_s - \mathcal{A} \mathbf{F}_s] - \kappa_p \rho_m \quad (64)$$

$$\mathbf{V}_s + \Lambda \mathbf{X}_s + \mathbf{A} \mathbf{F}_s = e^{-s\mathcal{T}} [\kappa_p (\mathbf{V}_m + \Lambda \mathbf{X}_m) - \mathcal{A} \kappa_f \mathbf{F}_m] - \rho_s. \quad (65)$$

Then, the stability of the teleoperation system under arbitrary time delay  $\mathcal{T} > 0$  can be ensured by satisfying the following sufficient condition,

$$\begin{cases} \|\mathcal{H}_{1s}(jw)^{-1} \mathcal{H}_{2s}(jw) \mathcal{H}_{1m}(jw)^{-1} \mathcal{H}_{2m}(jw)\|_{\infty} < 1, \\ \|\mathcal{H}_{1m}(jw)^{-1} \mathcal{H}_{2m}(jw) \mathcal{H}_{1s}(jw)^{-1} \mathcal{H}_{2s}(jw)\|_{\infty} < 1 \end{cases} \quad (66)$$

with,

$$\mathcal{H}_{1s}(s) \stackrel{\text{def}}{=} (s\mathbf{I} + \Lambda)(\mathcal{C}^{-1}s + \mathbf{I}_6) + s\mathcal{A}\mathbf{Z}_e(s) \quad (67)$$

$$\mathcal{H}_{2s}(s) \stackrel{\text{def}}{=} (s\mathbf{I} + \Lambda)\mathbf{I}_6 - s\mathcal{A}\kappa_f\kappa_p^{-1}\mathbf{Z}_h(s) \quad (68)$$

$$\mathcal{H}_{1m}(s) \stackrel{\text{def}}{=} (s\mathbf{I} + \Lambda)(\mathcal{C}^{-1}s + \mathbf{I}) + s\mathcal{A}\kappa_f\kappa_p^{-1}\mathbf{Z}_h(s) \quad (69)$$

$$\mathcal{H}_{2m}(s) \stackrel{\text{def}}{=} (s\mathbf{I} + \Lambda) - s\mathcal{A}\mathbf{Z}_e(s) \quad (70)$$

where  $\mathbf{Z}_e = F_s(s)/V_s(s)$  and  $\mathbf{Z}_h(s) = (F_m(s) - F_h(s))/V_m(s)$ . A simplified model for a single DoF system is derived in [44].

### B. Transparency

Substituting (54) and (55) into (23) and (52), one can obtain,

$$\begin{aligned} \rho_s + \kappa_p \rho_m &= -\mathcal{C}^{-1} \left( \kappa_p \dot{\mathbf{V}}_m + \dot{\mathbf{V}}_s + \Lambda (\kappa_p \mathbf{V}_m + \mathbf{V}_s) \right) \\ &\quad - 2\mathcal{A} (\mathbf{F}_s + \kappa_f \mathbf{F}_m). \end{aligned} \quad (71)$$

Then, substituting (60) and (61) in (71), one can have,

$$-\mathbf{F}_m = \kappa_f^{-1} \mathbf{F}_s + \kappa_f^{-1} \kappa_p \mathcal{A}^{-1} \mathcal{C}^{-1} (s\mathbf{I} + \Lambda) \mathbf{V}_m + \frac{1}{2} \kappa_f^{-1} \rho_1 \quad (72)$$

with

$$\rho_1 \stackrel{\text{def}}{=} \mathcal{A}^{-1} [\mathcal{C}^{-1} (s\mathbf{I} + \Lambda) (\rho_v) + (\rho_s + \kappa_p \rho_m)]. \quad (73)$$

On the other hand, from Fig. 5 following holds,

$$\mathbf{V}_s = -\frac{s}{s\mathbf{I} + \Lambda} \mathcal{A} \mathbf{F}_s + \kappa_p \mathbf{V}_m + \frac{s}{s\mathbf{I} + \Lambda} \rho_2 \quad (74)$$

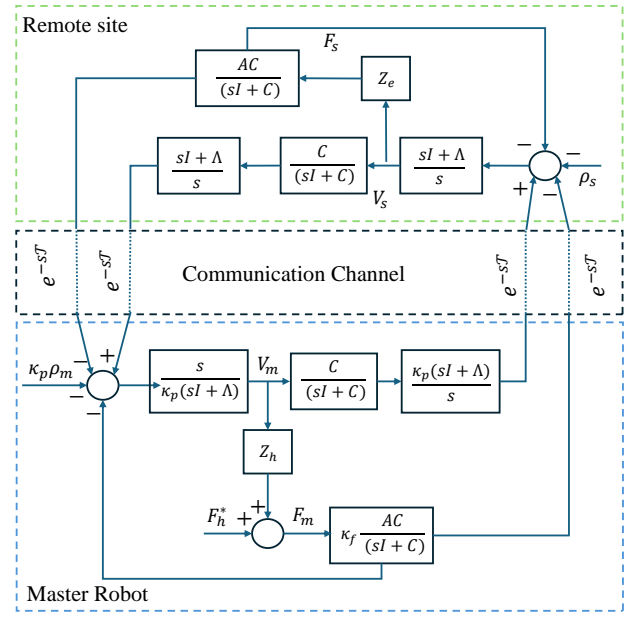


Fig. 5. Block diagram representation of dissimilar bilateral teleoperation with time delay

where,

$$\rho_2 \stackrel{\text{def}}{=} -\rho_s + \kappa_f [\rho_m - (V_{md} - V_m)]. \quad (75)$$

Then, (72) and (74) can be written in a compact form as,

$$\begin{bmatrix} -\mathbf{F}_m \\ -\mathbf{V}_s \end{bmatrix} = \underbrace{\begin{bmatrix} \kappa_f^{-1} \kappa_p \mathcal{A}^{-1} \mathcal{C}^{-1} (s\mathbf{I} + \Lambda) & \kappa_f^{-1} \\ -\kappa_p & \frac{s}{s\mathbf{I} + \Lambda} \mathcal{A} \end{bmatrix}}_G \begin{bmatrix} \mathbf{V}_m \\ \mathbf{F}_s \end{bmatrix} + \underbrace{\begin{bmatrix} \frac{1}{2} \kappa_f^{-1} \rho_1 \\ -\frac{s}{s\mathbf{I} + \Lambda} \rho_2 \end{bmatrix}}_{\rho}. \quad (76)$$

The  $G$  matrix in (76) is referred to as the transparency matrix. For high-fidelity bilateral teleoperation with motion/force scaling, the ideal transparency matrix is defined as [56]:

$$G_{\text{ideal}} = \begin{bmatrix} 0 & \kappa_f^{-1} \\ -\kappa_p & 0 \end{bmatrix}. \quad (77)$$

A comparison of the ideal transparency matrix in (77) with the actual matrix in (76) reveals that ideal transparency can be achieved when  $g_{11} = g_{12} = 0$ . However, this criterion is constrained by stability conditions. Consequently, perfect transparency and stability cannot be achieved simultaneously, and only a trade-off between the two can be satisfied. Nevertheless, by appropriately selecting the control gains, the transparency can be made close to ideal.

*Remark 3:* Nonzero values of  $g_{11}|_{\mathbf{F}_s=0}$  in (76) indicate that the operator may experience a sticky sensation while operating the master robot during free motion. Conversely, nonzero

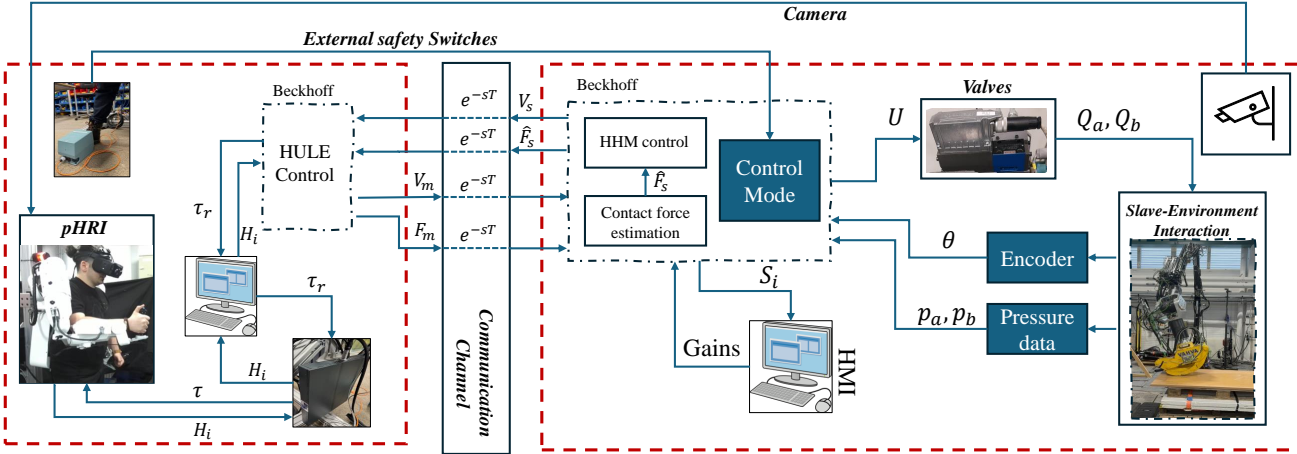


Fig. 6. Scheme of experiment setup; The teleoperation setup consists of master robot, master PC, master side Beckhoff, slave robot, slave PC, and slave side Beckhoff.

values of  $g_{11}|_{X_m=0}$  suggest that during contact between the slave robot and the environment—where the master robot remains stationary—the slave robot will move in response to environmental forces.

*Remark 4:* The term  $g_{11}$  in (76) represents the scaled impedance of the remote robot as perceived by the human arm when there is no contact force ( $\mathbf{F}_s = 0$ ). From  $g_{11}$ , it follows that,

$$\begin{aligned} \kappa_f^{-1} \kappa_p \mathcal{A}^{-1} \mathcal{C}^{-1} (s\mathbf{I} + \Lambda) \mathbf{V}_m &= \kappa_f^{-1} (\mathcal{A}^{-1} \mathcal{C}^{-1} (s\mathbf{I} + \Lambda)) \mathbf{V}_s \\ &= \kappa_f^{-1} \mathcal{A}^{-1} \mathbf{Z}_s, \end{aligned} \quad (78)$$

which indicates that during free motion, the force experienced by the human is equivalent to the scaled impedance of the remote robot. This concept is also illustrated in Fig. 1c.

## VII. EXPERIMENTAL RESULTS

This section is dedicated for comprehensive performance evaluation of the proposed method. Fig. 6 depicts the detail of the implementation setup. As can be seen, our experimental setup is a real-world benchmark designed to rigorously test the proposed control scheme under challenging conditions. The 7-DoF haptic exoskeleton master robot introduces inherent uncertainties from its complex forearm and wrist mechanisms, including belts, ball screws, and cables. These are compounded by the nonlinear fluid dynamics of the hydraulic actuators in the 6-DoF heavy-duty remote manipulator, along with potential UDP communication delays and packet loss. The human operator interacts with the system through virtual reality glasses, creating an immersive teleoperation experience that mirrors industrial applications. Such a unique configuration not only can challenge the adaptability of the control scheme to mechanical, hydraulic, and network complexities but also evaluates its potential universality and reliability in high-stakes, heavy-duty operations.

The entire teleoperation setup operates with a sample time of 1 ms. To ensure the safety of both the human operator and robots during teleoperation, a three-level safety mechanism is implemented, as illustrated in Fig. 6. First, in the user

interface, the operator selects the teleoperation mode, only after which the teleoperation is ready to be enabled. Then, the operator has to grab the handle of the exoskeleton, which with its sensing signals, the second phase is enabled and the algorithm is ready for the next. Finally, by pressing the pedal, which is an external signal to the control algorithm, the remote robots commands are linked to the master robot, or we can say, the teleoperation is enabled. By releasing either pedal or handle of the exoskeleton, the actuators of the exoskeleton are deactivated and the surrogate switches to its local control mode. Such a multi-level safety setup removes the risk of unaware teleoperation connection and potential damage to either robots or the operator. It must be emphasized that, prior to enabling teleoperation, all essential configurations, including control modes and gain adjustments, position and force scaling, and system calibration, are managed through a Human-Machine Interface (HMI) that has been entirely designed and developed in our laboratory using TwinCAT 3. This custom HMI is not a generic solution but a purpose-built interface, meticulously tailored to the unique requirements of our immersive bilateral teleoperation setup.

The conducted experiments consist of two main parts. The first part focuses on evaluating the performance of the proposed control algorithm under various conditions. Specifically, the algorithm is tested with different position and force scaling factors, which directly affect the operational velocity and contact force ranges, respectively, as well as under varying time delays. To comprehensively assess the performance of the control scheme, we define the following evaluation metrics:

- **Task Completion Time ( $\mathcal{T}$ ):** The total time required for the operator to execute the task illustrated in Fig. 7.
- **Maximum Tracking Error** of the displacement norm ( $\mathcal{N} = \|X_m\| - \|X_s\|$ ):

$$\mathcal{N}_{\max} = \max_{t \in [0, \mathcal{T}]} \mathcal{N}$$

- **Root Mean Square Error (RMSE) of the Displacement**

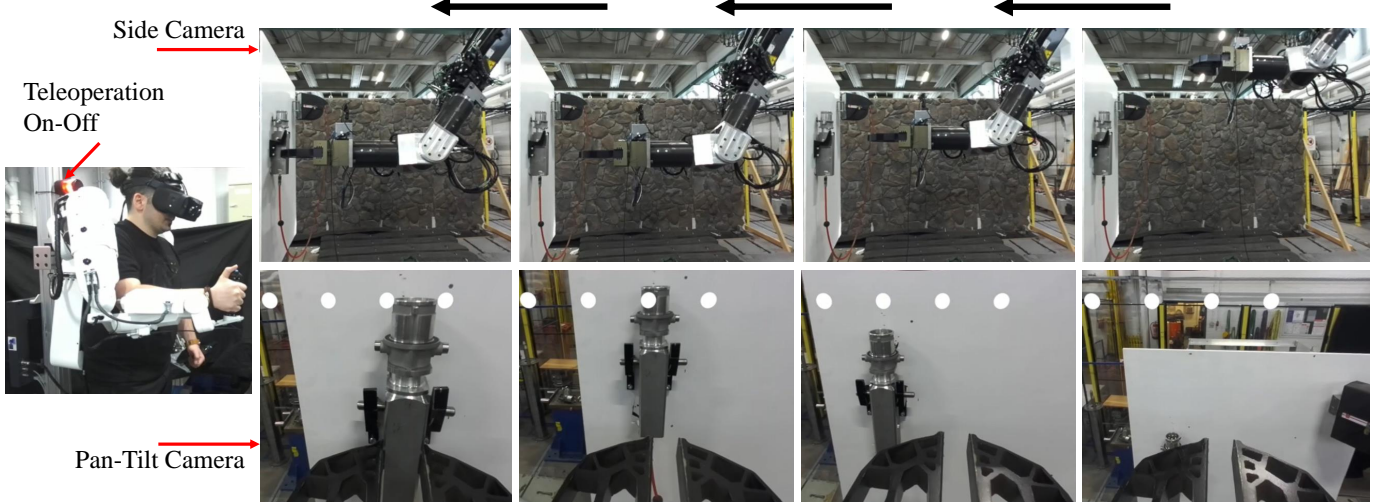


Fig. 7. Sequential steps of the free-motion experiment, shown from right to left. The remote robot, controlled by a human operator, approaches and grasps the target object. The top row displays the side camera view, while the bottom row shows the pan-tilt camera view—both providing essential visual feedback to support the operator's task execution.

**Norm ( $\mathcal{N}_{rms}$ ):**

$$\mathcal{N}_{rms} = RMS(\mathcal{N}) = \sqrt{\frac{1}{N} \sum_{i=1}^N \mathcal{N}_i^2}$$

- **Integral Absolute Error (IAE) of the Displacement Norm ( $\mathcal{N}_I$ ):**

$$\mathcal{N}_I = \int_0^{\mathcal{T}} |\mathcal{N}| dt$$

This metric captures the total accumulated deviation in position over the task duration.

- **Mean Absolute Error (MAE) of Velocity Tracking (V),** defined as the difference between the norm of the master and slave velocities:

$$\bar{V} = \frac{1}{N} \sum_{i=1}^N |V_i| = \frac{1}{N} \sum_{i=1}^N (||V_m|| - ||V_s||)$$

- **Position-Velocity Normalizing Index ( $\rho$ ),** which evaluates the relationship between the maximum position error and the maximum velocity:

$$\rho = \frac{|\mathcal{N}|_{\max}}{|V|_{\max}}$$

This index helps assess how well the slave robot can maintain accurate tracking under various velocity conditions.

- **Maximum and RMS of Force Tracking Error ( $\mathcal{F}_{\max}, \mathcal{F}_{rms}$ ),** representing the instantaneous and average discrepancy between the master-side commanded force and the slave-side estimated contact force in the direction of interaction with  $\mathcal{F} = F_m(t) - F_s(t)$ :

$$\mathcal{F}_{\max} = \max_{t \in [0, \mathcal{T}]} |\mathcal{F}|, \quad \mathcal{F}_{rms} = RMS(\mathcal{F})$$

These metrics ensure a detailed and robust evaluation of the proposed control scheme under different scaling, time delay, and contact conditions. In the second set of experiments,

we conducted a user study to evaluate the performance and usability of the proposed control scheme, the detail of which is provided in subsection VII-C.

In all experiments, the filter constant was set to  $\mathcal{C} = 35$ . For experiments without time delay, the force and position control gains were set to  $\mathcal{A} = 80 \times 10^{-5}$  and  $\Lambda = 12$ , respectively. In contrast, for experiments involving communication delay, the gains were adjusted to  $\mathcal{A} = 50 \times 10^{-5}$  and  $\Lambda = 3$  to satisfy the stability condition defined in (66), thereby achieving an optimal trade-off between maximum tolerable fixed delay and acceptable control accuracy. For the user study experiments, the control gains were set to  $\mathcal{A} = 80 \times 10^{-5}$  and  $\Lambda = 4$  to ensure smooth interaction and allow the remote robot to tolerate fast and high-jerk commands from participants, who were non-expert teleoperators. The local control gains for both the master and surrogate systems were configured identically to those reported in [51] and [52].

#### A. Free Motion Performance Evaluation

In this section, we evaluate the controller's performance under different motion scaling conditions. In particular, we investigate three representative scale factors: low ( $\kappa_p = 1$ ), medium ( $\kappa_p = 7$ ), and high ( $\kappa_p = 13$ ). During each trial, the operator is instructed to approach a designated task board (Fig. 5), align the end-effector with the object of interest, and perform a grasping operation. The complete sequence of this free-motion task is illustrated in Fig. 7, enabling a visual comparison of system behavior under different scaling settings. The experimental results are presented in Fig. 8. Figs. 8a–8c plot the norm of the end-effector position for each scale, while Figs. 8d–8f show the corresponding velocity norms. Across all cases, the proposed controller demonstrates stable tracking and accurate translation of the operator's commands to the slave robot.

Under  $\kappa_p = 1$ , the operator required multiple indexing motions to reach the goal, primarily due to the mismatch

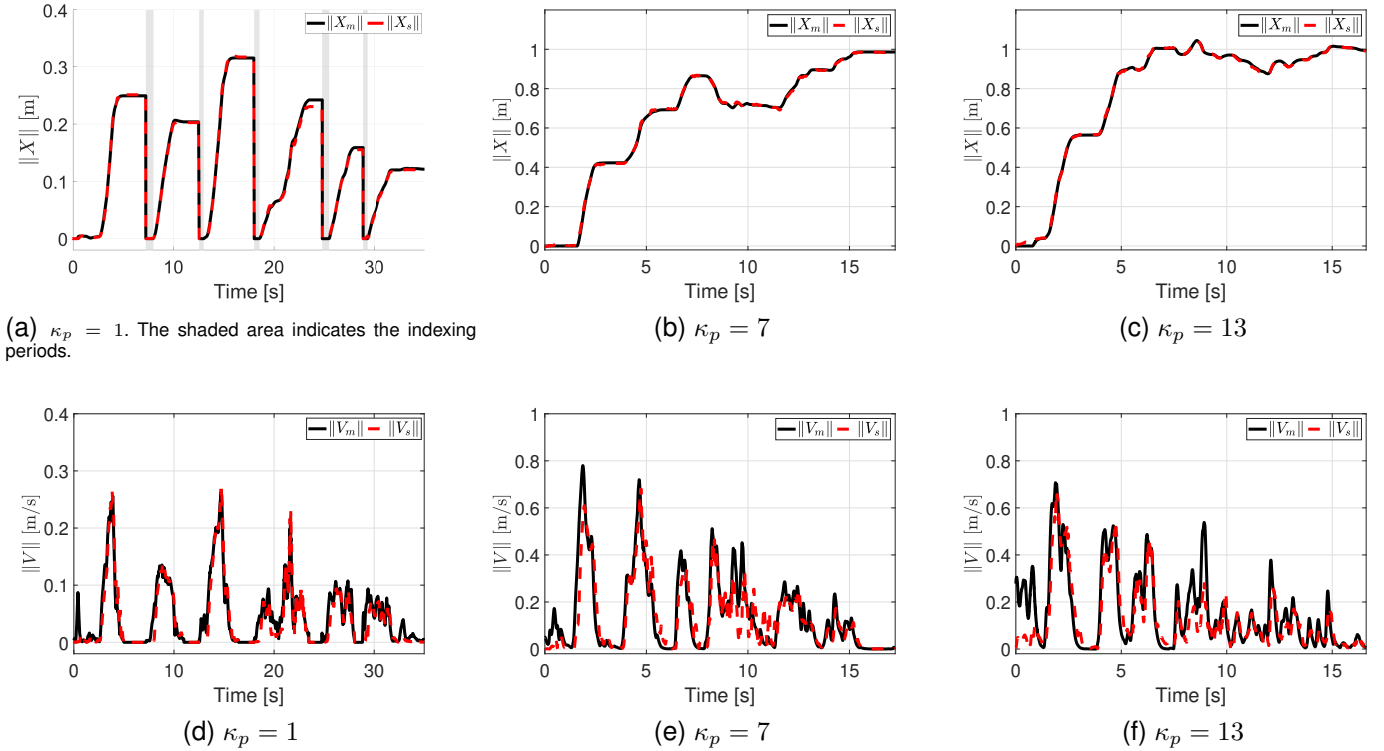


Fig. 8. Experimental results of the free-motion task under different motion scaling factors. Subfigures (a)–(c) show the norm of position tracking, while subfigures (d)–(f) present the norm of velocity tracking.

TABLE I  
PERFORMANCE METRICS FOR DIFFERENT POSITION AND ORIENTATION SCALING FACTORS.

Experiments	$\mathcal{T}$ [s]	$\mathcal{N}_{p,\max}$ [m]	$\mathcal{N}_{p,rms}$ [m]	$\mathcal{N}_{p,I}$ [m·s]	$\bar{V}$ [m/s]	$\rho$	$\mathcal{N}_{o,\max}$ [deg]	$\mathcal{N}_{o,rms}$ [deg]
$\kappa_p = 1$	35	0.011	0.0037	0.093	0.011	0.043	0.94	0.34
$\kappa_p = 7$	17.25	0.020	0.0052	0.068	0.04	0.03	0.820	0.43
$\kappa_p = 13$	16.6	0.029	0.0057	0.064	0.056	0.044	0.76	0.43
<i>Experiments below are conducted with delay and <math>\kappa_p = 3</math>:</i>								
Fixed delay $\mathcal{T}_f = 150$ ms	16.6	0.029	0.0057	0.064	0.056	0.044	0.76	0.43
Time-varying delay $0 < \mathcal{T}_v < 150$ ms	16.6	0.029	0.0057	0.064	0.056	0.044	0.76	0.43

between the limited workspace of the human arm and the extended reach of the remote manipulator. In contrast, with higher scaling factors, the operator could traverse larger distances on the slave side with smaller physical inputs. However, this increased mobility came at a perceptual cost. As the scale rose from 7 to 13, operator experienced a temporary mismatch between their proprioceptive sense of motion and the observed robot behavior through VR, which resulted in a longer time to think about how to accomplish the task. This phenomenon is evident in the only marginal improvement in execution time between  $\kappa_p = 7$  and  $\kappa_p = 13$ , despite the latter offering greater kinematic amplification. We posit that the observed discrepancy in perceptual adaptation stems from a form of sensorimotor mismatch: while the operator consciously understands the presence of motion scaling, their sensorimotor system temporarily resists reconciling slow proprioceptive input with fast visual feedback from the robot. Such dissonance, though initially disruptive, appears to diminish with exposure and may be mitigated further by brief adaptation phases or

gradual scale ramping.

Table I quantifies these observations. As expected, task execution time  $\mathcal{T}$  decreases with increasing scale due to faster end-effector velocities. However, the position tracking error increases accordingly: maximum error rises from 1.1 cm to 2.9 cm, and RMS error from 0.37 cm to 0.57 cm, as  $\kappa_p$  increases from 1 to 13. Despite this, the velocity-normalized error index  $\rho$  remains relatively consistent across all experiments, indicating that the tracking accuracy scales proportionally with motion speed, and the controller maintains a well-balanced performance. Furthermore, the controller maintained excellent velocity and orientation tracking performance, even under the high accelerations and velocities induced by large motion scaling factors in such a heavy-duty system.

To assess delay robustness, we introduce communication latency into the loop. Fig. 9 presents results from experiments involving a fixed one-way delay of  $\mathcal{T}_f = 150$  ms (Fig. 9a) and a bounded, time-varying delay with  $0 < \mathcal{T}_v < 150$  ms (Fig. 9b) all with  $\kappa_p = 3$ . The variable delay was generated using a

uniformly distributed random process. In both scenarios, the system remains stable and task completion is achieved with acceptable accuracy. Quantitative metrics reported in Table I confirm that, although performance degrades modestly under delay, the controller maintains operational transparency and remains responsive to the human operator's commands.

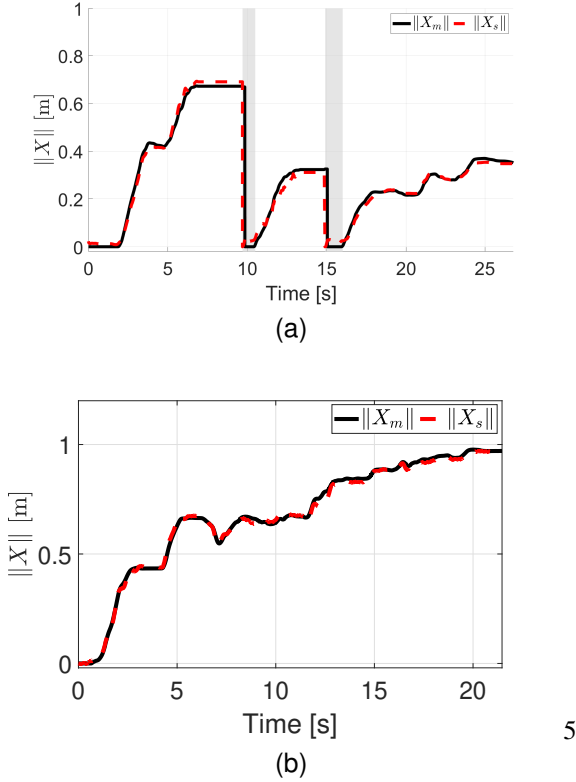


Fig. 9. Performance evaluation of the teleoperation system under delayed conditions. (a) Fixed communication delay  $T_f = 150$  ms. (b) Time-varying delay  $0 < T_v < 150$  ms.

To further evaluate the performance of the proposed controller, the operator was instructed to perform a random motion in space, commanding both position and orientation changes of the end-effector. The results of this experiment with a scaling factor of  $\kappa_p = 4$  are illustrated in Fig. 10. Specifically, Fig. 10a displays the end-effector position trajectories, Fig. 10b shows the orientation tracking in terms of Euler angles, Fig. 10c presents the quaternion RMS error, Fig. 10d depicts the position RMS error, and Fig. 10e shows the norm of the end-effector velocity. The results demonstrate the excellent tracking performance of the proposed controller, with orientation errors remaining below 2deg and position errors within 2 cm.

### B. Contact-rich Performance

In this section, the force-reflection and force-tracking capabilities of the teleoperation system are evaluated. To assess these functionalities, the operator was instructed to drive the remote robot, establish contact with a remote object, and then apply interaction forces upon sensing contact. The experimental procedure is illustrated in Fig. ???. These experiments were conducted with a motion scaling factor of  $\kappa_p = 2$  and varying

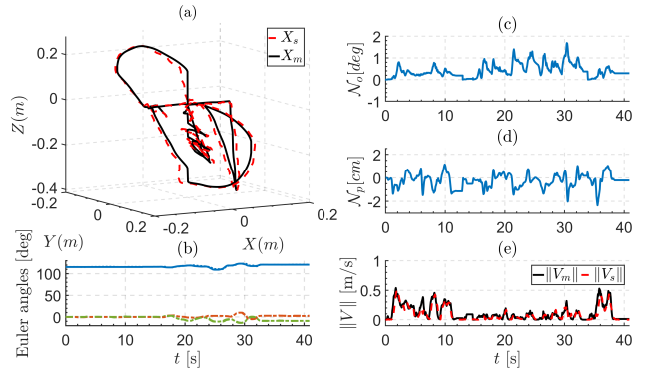


Fig. 10. Block diagram representation of dissimilar bilateral teleoperation with time delay

force scaling values of  $\kappa_f = 500, 800$ , and  $1000$ . The results are presented in Fig. 11. As shown, the forces applied by the operator are effectively transmitted through the system and exerted on the remote environment with high fidelity. These results demonstrate that human-applied forces can be amplified up to 1000 times, which is a significant achievement.

In addition, contact experiments were conducted in the presence of both fixed and time-varying communication delays, using a force scaling factor of  $\kappa_f = 800$ . The results are shown in Fig. 12: Fig. 12a presents position and force tracking under a fixed delay, while Fig. 12b shows the same under a time-varying delay. These delayed experiments were performed over extended durations compared to the non-delayed ones to further investigate system stability and transparency. Despite the presence of considerable communication delay, the proposed control scheme maintained a favorable trade-off between transparency and stability.

A quantitative summary of the results is provided in Table II. For instance, with  $\kappa_f = 500$ , the maximum and RMS force errors reached 737 N and 387 N, respectively. When the force scaling was increased to  $\kappa_f = 1000$ , the maximum and RMS errors remained comparable at 848 N and 448 N, respectively—indicating robust tracking performance even under extreme amplification. As expected, the addition of delay degraded tracking performance to some extent. Nevertheless, the controller maintained stable execution and preserved a strong sense of transparency. Other metrics reported in Table II, such as position and orientation errors, further confirm the excellent performance of the controller in both delayed and non-delayed conditions.

### C. User Study

To evaluate the SoE and usability of the proposed teleoperation system, we conducted a user study using an adapted version of the questionnaire from [57] for SoE assessment, alongside a custom-designed questionnaire to evaluate system usability. A total of 10 participants (9 male, 1 female) were recruited, shown in Fig. 13, and instructed to complete the same free motion task illustrated in Fig. 7 with  $\kappa_p = 2$ . To intentionally challenge the system's robustness under non-expert operation, the training phase was deliberately minimal.

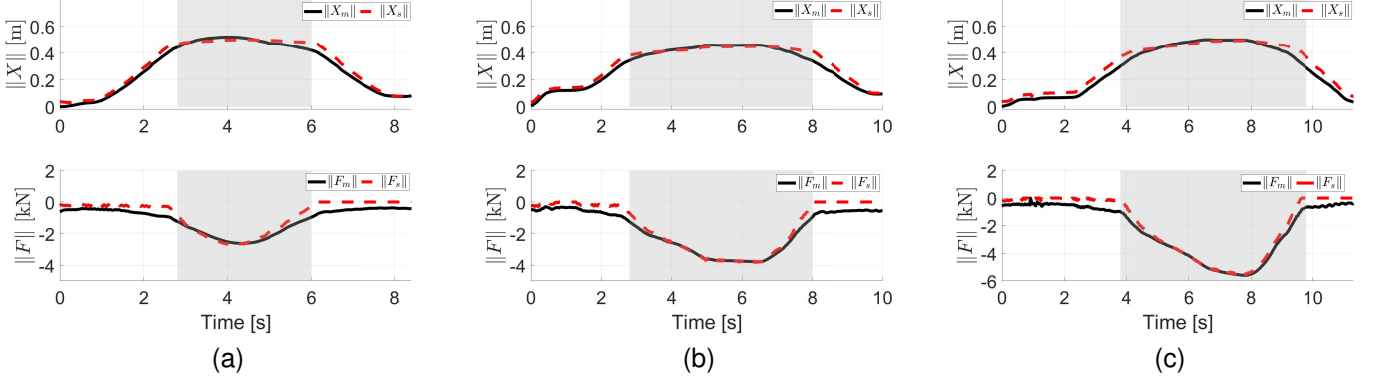


Fig. 11. Comparison of position and velocity tracking in three cases.

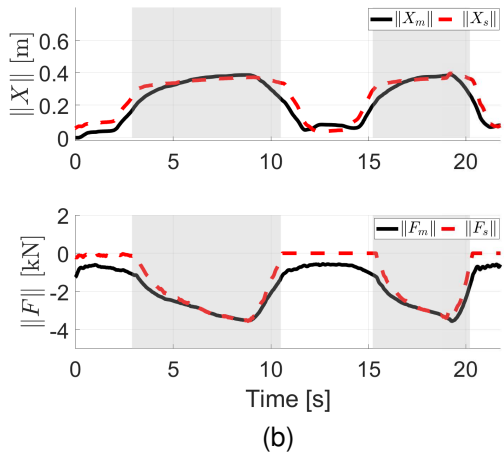
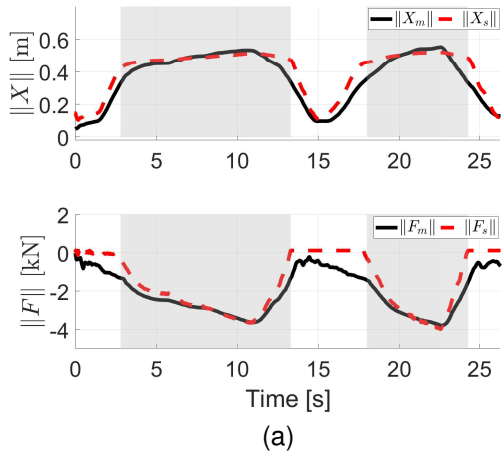


Fig. 12. Comparison of position and velocity tracking in three cases.

Participants were briefly introduced to the system, including expected haptic and visual feedback, and were then given only 2–3 minutes to familiarize themselves with the haptic exoskeleton through self-guided exploration. The ability of novice users to operate a heavy-duty hydraulic manipulator via a high-fidelity teleoperation interface with such limited familiarization time is highly significant. This level of accessibility

TABLE II  
PERFORMANCE METRICS IN CONTACT TASKS UNDER DIFFERENT FORCE SCALING AND DELAY CONDITIONS.

Experiments	$\mathcal{N}_{p,\text{rms}}$ [m]	$\mathcal{N}_{o,\text{rms}}$ [deg]	$\mathcal{F}_{\text{max}}$ [N]	$\mathcal{F}_{\text{rms}}$ [N]
$k_f = 500$	0.0302	0.52	737.79	387.90
$k_f = 800$	0.0299	0.51	779.00	391.65
$k_f = 1000$	0.0408	0.45	848.60	448.25
<i>Experiments below are conducted with delay and <math>\kappa_f = 800</math>:</i>				
$\mathcal{T}_f = 150$ ms	0.0597	0.75	1638.73	676.80
$0 < \mathcal{T}_v < 150$ ms	0.0508	0.74	1171.71	588.88

is rarely reported in the literature, particularly for bilateral teleoperation systems involving real-world hydraulic actuators, which are typically characterized by nonlinearities, delays, and high inertial dynamics. To the best of our knowledge, very few—if any—existing studies have demonstrated comparable usability in such complex settings.

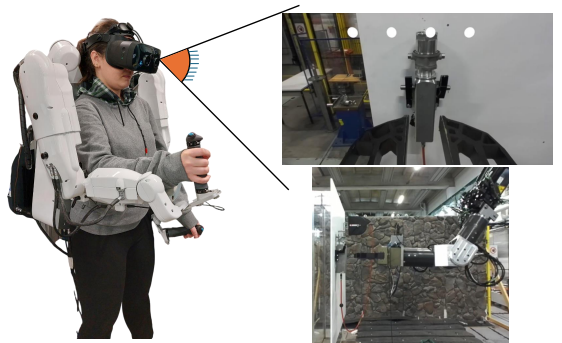


Fig. 13. User study experiment. The user is tasked to grasp the object on the what board.

The participant pool included individuals with varying anthropometric profiles, particularly in height, thereby allowing us to assess the ergonomic and functional adaptability of the teleoperation setup across different operator physiques and genders. This diversity supports the generalizability of the proposed interface for a broad user population. Following the brief familiarization session, each participant performed the

actual teleoperation task using the proposed setup. During this phase, the same objective performance metrics as in the prior experiments were recorded to enable quantitative evaluation of task execution. At the conclusion of the experiment, participants completed a standardized 7-point Likert-scale questionnaire (1 = strongly disagree, 7 = strongly agree) designed to assess three core subjective dimensions:

- **Sense of Agency (SoA):** The participant's perception of being in control of the slave robot's movements.
- **Sense of Self-Location (SoSL):** The perceived spatial presence at the location of the remote robot.
- **Sense of Ownership (SoO):** The extent to which the remote robot was experienced as part of the participant's own body.
- **System Usability:** The perceived intuitiveness and ease of use of the teleoperation interface.

Although SoO was not a primary focus of this study, we included one item related to ownership to explore whether high SoA and SoSL might induce a partial sense of embodiment. The completed questionnaire is provided in Table III.

TABLE III  
QUESTIONNAIRE ITEMS FOR ASSESSING SOA, SOSL, OWNERSHIP, AND USABILITY

Question	Statement	Score
<b>Category A: Sense of Agency</b>		
$Q_{A_1}$	It felt like I could control the remote arm as if it was my own arm.	$5.20 \pm 0.79$
$Q_{A_2}$	The movements of the remote arm were caused by my movements.	$6.50 \pm 0.71$
$Q_{A_3}$	I felt as if the movements of the remote arm were influencing my own movements.	$4.90 \pm 1.29$
$Q_{A_4}$	I felt as if the remote arm was moving by itself.	$1.60 \pm 0.70$
<b>Category L: Sense of Self-Location</b>		
$Q_{L_1}$	I felt as if I were located where the remote robot was.	$5.40 \pm 0.70$
$Q_{L_2}$	It felt as if I was seeing the environment through the eyes of the remote robot.	$6.00 \pm 0.82$
$Q_{L_3}$	I felt as if I was looking around the environment with my own head movements.	$6.10 \pm 1.20$
<b>Category O: Sense of Ownership</b>		
$Q_{O_1}$	I felt the remote body as if it were part of my own body.	$4.90 \pm 0.99$
$Q_{O_2}$	I felt the remote body as an extension of my own body.	$4.90 \pm 1.20$
<b>Category U: Usability</b>		
$Q_{U_1}$	I found the system very difficult to use.	$2.00 \pm 0.47$
$Q_{U_2}$	I felt comfortable using the system.	$5.70 \pm 0.82$
$Q_{U_3}$	I felt very confident using the system.	$6.10 \pm 0.88$
$Q_{U_4}$	The task required a lot of mental effort.	$2.70 \pm 1.34$

The results of the questionnaire in Table III highlight the effectiveness of the proposed teleoperation setup in inducing a strong sense of agency, self-location, and usability—despite the system's complexity and dissimilarity along with short familiarization period provided to the participants. Notably, participants reported a high level of control over the remote manipulator ( $Q_{A_2} = 6.50 \pm 0.71$ ) and a very low agree-

ment with the statement that the robot moved autonomously ( $Q_{A_4} = 1.60 \pm 0.70$ ), indicating a robust sense of agency. Additionally, responses to  $Q_{A_1}$  and  $Q_{A_3}$  indicate that participants not only felt in control of the remote arm, but also experienced a tangible connection between their actions and the robot's movements, likely facilitated by the distribution of scaled impedance of remote arm onto their own via the haptic exoskeleton. The high scores in the self-location category (e.g.,  $Q_{L_2} = 6.00 \pm 0.82$ ,  $Q_{L_3} = 6.10 \pm 1.20$ ) demonstrate that participants strongly felt as if they were spatially co-located with the remote robot. This is especially noteworthy given the asymmetry between the human operator's body and the heavy-duty hydraulic manipulator, and it can be attributed to the use of egocentric viewpoint tracking and immersive VR headsets. Although inducing a sense of ownership was not a primary objective, the responses to  $Q_{O_1}$  and  $Q_{O_2}$  (4.9 average) indicate that a moderate level of embodiment was achieved. This is likely a result of the enhanced agency and self-location, both of which are known precursors to ownership in embodiment research. Interestingly, participants rated both the perception of the robot as a part of their body and as an extension of their body nearly equally, suggesting a nuanced experience of embodiment. To derive an overall measure of the established level of SoE, the participants' questionnaire responses were linearly scaled to a normalized range of 0–100. As a result, the average normalized SoE score across all participants was found to be 76.4%, indicating a notably high level of embodiment. This is a particularly strong outcome considering the substantial dissimilarity and dynamic complexity of the master–slave system used in the experiments.

The usability results are particularly significant. Despite the use of a large-scale, heavy-duty slave manipulator, participants reported high comfort ( $Q_{U_2} = 5.70 \pm 0.82$ ) and confidence ( $Q_{U_3} = 6.10 \pm 0.88$ ) with low perceived difficulty ( $Q_{U_1} = 2.00 \pm 0.47$ ) and mental effort ( $Q_{U_4} = 2.70 \pm 1.34$ ). These scores underscore the intuitiveness and accessibility of the system—even for users with no prior experience without limitation to gender—further validating the ergonomic and cognitive effectiveness of the proposed control and interface design. Importantly, these subjective outcomes were achieved with a minimal familiarization session of only 2–3 minutes. Taken together, these findings provide compelling evidence for the system's effectiveness in supporting natural, intuitive, and immersive control, even in complex and non-anthropomorphic teleoperation scenarios.

To complement the subjective assessment, objective performance metrics are summarized in Table IV. The maximum position tracking error was limited to 2.88 cm, with an RMS error of 1.1 cm, and orientation tracking remained excellent throughout. The mean end-effector velocity tracking error was 0.058 m/s, with an average task execution time of 22.8 s. Notably, these results were achieved despite reducing the position control gain  $\Lambda$  from 12 (used in optimal no-delay conditions) to 4—i.e., only 33% of the nominal gain. This confirms that the controller preserves stability even with significantly reduced gains, and that gain tuning primarily affects performance rather than stability. This is especially important in user studies,

where robustness to suboptimal and variable commands from non-expert operators is essential. These findings further validate the system's real-world applicability and resilience.

TABLE IV  
OBJECTIVE METRICS FROM USER STUDY EXPERIMENTS

Metric	Mean $\pm$ Std
$\mathcal{N}_{p,\max}$ [cm]	2.88 $\pm$ 0.96
$\mathcal{N}_{p,\text{rms}}$ [cm]	1.09 $\pm$ 0.36
$\mathcal{N}_{o,\max}$ [deg]	1.10 $\pm$ 0.12
$\mathcal{N}_{o,\text{rms}}$ [deg]	0.66 $\pm$ 0.05
$\mathcal{N}_{v,\text{rms}}$ [m/s]	0.058 $\pm$ 0.016
$\mathcal{T}$ [s]	22.8 $\pm$ 8.9

### VIII. CONCLUSION

This study presented an immersive bilateral teleoperation framework with force reflection, tailored for highly dissimilar master–slave systems without relying on physical force sensors. To address the fundamental challenge of human engagement in such teleoperation scenarios, we focused on enhancing the operator's Sense of Embodiment (SoE), specifically targeting the Sense of Agency (SoA) and Sense of Self-Location (SoSL). High transparency was achieved through a robust and accurate control design capable of handling model uncertainties, input nonlinearities, and arbitrary time delays. Immersion was reinforced using a wearable haptic exoskeleton for distributed force rendering and a VR headset with egocentric head tracking to establish telepresence. Theoretical analysis confirmed the semi-global uniform ultimate boundedness of the closed-loop system. Extensive real-world experiments validated the controller's robustness and performance across a wide range of motion and force scaling conditions, including up to 1:13 motion scaling and 1:1000 force scaling, both with and without fixed or time-varying communication delays up to 150 ms. Additionally, a comprehensive user study demonstrated the system's capability to elicit high SoE across all participants, with normalized embodiment scores 76.4%, regardless of gender-specific limitations. Participants also found the interface intuitive and easy to use, a noteworthy outcome given the scale and dynamics of the heavy-duty remote manipulator.

While this work provides a strong foundation for immersive teleoperation in large-scale robotic systems, several enhancements remain. A promising future direction includes mapping detected contact points on the remote robot to anatomically equivalent regions on the human body, enhancing contextual awareness and embodiment. Optimizing the location and control of the pan-tilt camera system may further reinforce first-person perspective and spatial congruence. Finally, integrating learning-from-demonstration techniques could facilitate skill transfer from humans to machines, advancing the autonomy of heavy-duty systems beyond current human capabilities.

### APPENDIX A UPPER BOUND OF $p_{T_7}$

In the context of VDC, the augmented velocity is defined as,

$$\mathcal{V} = \mathcal{J} \dot{q} \quad (A.1)$$

where  $\mathcal{J}$  is the augmented Jacobian matrix that maps the joint velocities vector to the augmented velocity vector. The  $\mathcal{V}$  contains all the velocities of the frames of the entire decomposed system (for more detail refer to [58, Section 3.3.5]). In the same sense, we can write the following that maps the augmented net force vectors to the actuator torque vector,

$$\tau = \mathcal{J}^T \mathcal{F}. \quad (A.2)$$

Exploiting (A.1) and (A.2), the following can be reconstructed for arm dynamics from (6)–(8),

$$\tau_m = \mathcal{J}^T \mathcal{M} \mathcal{J} \ddot{q} + \mathcal{J}^T \mathcal{M} \mathcal{J} \dot{q} + \mathcal{J}^T \mathcal{C} \quad (A.3)$$

with  $M_h \in \mathbb{R}^{6 \times 6}$ ,  $C_h \in \mathbb{R}^{6 \times 6}$ ,  $G_h \in \mathbb{R}^{6 \times 6}$  being mass, damping, and stiffness matrices of human arm,  $\tau_h \in \mathbb{R}^6$  being human exogenous torque, and  $\tau_m \in \mathbb{R}^6$  being applied torque from master robot to human arm. In the same sense, we can write,

$$\tau_{mr} = \mathcal{J}^T \hat{\mathcal{M}} \mathcal{J} \ddot{q}_r + \mathcal{J}^T \hat{\mathcal{M}} \mathcal{J} \dot{q} + \mathcal{J}^T \hat{\mathcal{C}}. \quad (A.4)$$

The linear-in-parameter form for (A.4) can be written as below,

$$\mathcal{Y}_e \Phi_e = \mathcal{J}^T \hat{\mathcal{M}} \mathcal{J} \ddot{q}_r + \mathcal{J}^T \hat{\mathcal{M}} \mathcal{J} \dot{q} + \mathcal{J}^T \hat{\mathcal{C}}. \quad (A.5)$$

By adding and subtracting  $\mathcal{J}^T \mathcal{M} \mathcal{J} \ddot{q}_r$  to the right hand side of (A.3) and substituting in  $(\tau_{mr} - \tau_m)$ , one can establish.

$$\tau_{hr} - \tau_h = \mathcal{Y}_e (\hat{\Phi}_e - \Phi_e) + \mathcal{J}^T \mathcal{M} \mathcal{J} (\ddot{q}_r - \ddot{q}) + \hat{\tau}_h^* - \tau_h^*. \quad (A.6)$$

On the other hand, for the VPF of the frame  $\{T_7\}$  of the master robot, we can write,

$$\begin{aligned} p_{T_7} &= ({}^{T_7}V_r - {}^{T_7}V)^T ({}^{T_7}F_r - {}^{T_7}F) \\ &= (\dot{X}_{hr} - \dot{X}_{hr})^T (F_{mr} - F_m). \end{aligned} \quad (A.7)$$

During the physical human-robot interaction,  $p_{T_7}$  represents the power injected or absorbed by human operator. Additionally, during the interaction phase, as human grasping the handle of exoskeleton, there is always a flow of power between robot and human arm, indicating  $\|p_{T_7}\| \leq \varrho_m$  with  $\varrho_m > 0$  is small constant. Then, by assuming that  $\dot{X}_{hr} = V_{mr}$  and  $\dot{X}_h = V_m$  along with using  $\dot{q}_r = J^{-1}V_{mr}$ , one can obtain,

$$p_{T_7} = (\dot{q}_r - \dot{q})^T (\tau_{hr} - \tau_h). \quad (A.8)$$

Then, by replacing from (A.6) in (A.8), we have,

$$\begin{aligned} p_{T_7} &= (\dot{q}_r - \dot{q})^T \mathcal{Y}_e (\hat{\Phi}_e - \Phi_e) \\ &= (\dot{q}_r - \dot{q})^T \mathcal{J}^T \mathcal{M} \mathcal{J} (\ddot{q}_r - \ddot{q}) \\ &= (\dot{q}_r - \dot{q})^T (\hat{\tau}_h^* - \tau_h^*). \end{aligned} \quad (A.9)$$

Taking the integral of the  $p_{T7}$  as below,

$$\begin{aligned} \lim_{t \rightarrow \infty} \int_0^t p_{T7} dt &= \lim_{t \rightarrow \infty} \int_0^t (\dot{q}_r - \dot{q})^T \mathcal{Y}_e (\hat{\Phi}_e - \Phi_e) \\ &\quad + \lim_{t \rightarrow \infty} \int_0^t (\dot{q}_r - \dot{q})^T \mathcal{J}^T \mathcal{M} \mathcal{J} (\ddot{q}_r - \ddot{q}) \\ &\quad + \lim_{t \rightarrow \infty} \int_0^t (\dot{q}_r - \dot{q})^T (\hat{\tau}_h^* - \tau_h^*). \end{aligned} \quad (\text{A.10})$$

yields to,

$$\begin{aligned} \lim_{t \rightarrow \infty} \int_0^t p_{T7} dt &\geq -\frac{\gamma}{2} \tilde{\Phi}_e(0) \Gamma(\hat{\Phi}(0)) \tilde{\Phi}_e(0) \\ &\quad - \frac{1}{2} (\dot{q}_r(0) - \dot{q}(0))^T \mathcal{J}^T \mathcal{M} \mathcal{J} (\dot{q}_r(0) - \dot{q}(0)) \\ &\geq -\varrho_{0m} \end{aligned} \quad (\text{A.11})$$

with,

$$\begin{aligned} \varrho_{0m} &= \frac{\gamma}{2} \tilde{\Phi}_e(0) \Gamma(\hat{\Phi}(0)) \tilde{\Phi}_e(0) \\ &\quad + \frac{1}{2} (\dot{q}_r(0) - \dot{q}(0))^T \mathcal{J}^T \mathcal{M} \mathcal{J} (\dot{q}_r(0) - \dot{q}(0)). \end{aligned} \quad (\text{A.12})$$

where  $\Gamma(\hat{\Phi}_h(0))$  is the constant pullback of Riemannian metric [53].

## APPENDIX B PROOF OF LEMMA 5

By employing Definition 1, (40) and (46) along with  $V_s = V_T$ , the following holds for  $p_T$ ,

$$\begin{aligned} p_T &= ({}^T V_r - {}^T V)^T ({}^T F_r - {}^T F) \\ &= ({}^T V_r - {}^T V)^T N_c (f_{ed} - f_e) \\ &= ({}^T V_r - {}^T V)^T N_c M_e (\dot{V}_{sr} - \dot{V}_s) \\ &= (V_{sr} - V_s)^T M_e (\dot{V}_{sr} - \dot{V}_s) \end{aligned} \quad (\text{B.1})$$

which leads to,

$$\begin{aligned} \int_0^\infty p_T dt &= \int_0^\infty (V_{sr} - V_s)^T M_e (V_{sr} - V_s) dt \\ &\geq -0.5 (V_{sr}(0) - V_s(0))^T M_e (\dot{V}_{sr}(0) - \dot{V}_s(0)) \\ &\geq -\varrho_{0s}. \end{aligned} \quad (\text{B.2})$$

## REFERENCES

- [1] P. F. Hokayem and M. W. Spong, "Bilateral teleoperation: An historical survey," *Automatica*, vol. 42, no. 12, pp. 2035–2057, 2006.
- [2] H. Chen, P. Huang, and Z. Liu, "Mode switching-based symmetric predictive control mechanism for networked teleoperation space robot system," *IEEE/ASME Transactions on Mechatronics*, vol. 24, no. 6, pp. 2706–2717, 2019.
- [3] H. Su, C. Yang, G. Ferrigno, and E. De Momi, "Improved human-robot collaborative control of redundant robot for teleoperated minimally invasive surgery," *IEEE Robotics and Automation Letters*, vol. 4, no. 2, pp. 1447–1453, 2019.
- [4] M. Selvaggio, J. Cacace, C. Pacchierotti, F. Ruggiero, and P. R. Giordano, "A shared-control teleoperation architecture for nonprehensile object transportation," *IEEE Transactions on Robotics*, vol. 38, no. 1, pp. 569–583, 2021.
- [5] M. Suomalainen, J. Koivumäki, S. Lampinen, V. Kyrki, and J. Mattila, "Learning from demonstration for hydraulic manipulators," in *2018 IEEE/RSJ International Conference on Intelligent Robots and Systems (IROS)*. IEEE, 2018, pp. 3579–3586.
- [6] J. Mattila, J. Koivumäki, D. G. Caldwell, and C. Semini, "A survey on control of hydraulic robotic manipulators with projection to future trends," *iEeE/ASME Transactions on Mechatronics*, vol. 22, no. 2, pp. 669–680, 2017.
- [7] J. Zhang, E. Langbehn, D. Krupke, N. Katzakis, and F. Steinicke, "Detection thresholds for rotation and translation gains in 360 video-based telepresence systems," *IEEE transactions on visualization and computer graphics*, vol. 24, no. 4, pp. 1671–1680, 2018.
- [8] M. Slater and S. Wilbur, "A framework for immersive virtual environments (five): Speculations on the role of presence in virtual environments," *Presence: Teleoperators & Virtual Environments*, vol. 6, no. 6, pp. 603–616, 1997.
- [9] S. R. Ellis, "Presence of mind: a reaction to thomas sheridan's 'further musings on the psychophysics of presence,'" *Presence: Teleoperators & Virtual Environments*, vol. 5, no. 2, pp. 247–259, 1996.
- [10] E. B. Nash, G. W. Edwards, J. A. Thompson, and W. Barfield, "A review of presence and performance in virtual environments," *International Journal of human-computer Interaction*, vol. 12, no. 1, pp. 1–41, 2000.
- [11] M. Slater, "Place illusion and plausibility can lead to realistic behaviour in immersive virtual environments," *Philosophical Transactions of the Royal Society B: Biological Sciences*, vol. 364, no. 1535, pp. 3549–3557, 2009.
- [12] K. Kiltani, R. Groten, and M. Slater, "The sense of embodiment in virtual reality," *Presence: Teleoperators and Virtual Environments*, vol. 21, no. 4, pp. 373–387, 2012.
- [13] S. Falcone, G. Englebienne, J. Van Erp, and D. Heylen, "Toward standard guidelines to design the sense of embodiment in teleoperation applications: A review and toolbox," *Human–Computer Interaction*, vol. 38, no. 5–6, pp. 322–351, 2023.
- [14] M. E. Cabrera and J. P. Wachs, "A human-centered approach to one-shot gesture learning," *Frontiers in Robotics and AI*, vol. 4, p. 8, 2017.
- [15] D. Wei, B. Huang, and Q. Li, "Multi-view merging for robot teleoperation with virtual reality," *IEEE Robotics and Automation Letters*, vol. 6, no. 4, pp. 8537–8544, 2021.
- [16] X. Cheng, J. Li, S. Yang, G. Yang, and X. Wang, "Open-television: Teleoperation with immersive active visual feedback," *arXiv preprint arXiv:2407.01512*, 2024.
- [17] V. Girbes-Juan, V. Schettino, Y. Demiris, and J. Tornero, "Haptic and visual feedback assistance for dual-arm robot teleoperation in surface conditioning tasks," *IEEE Transactions on Haptics*, vol. 14, no. 1, pp. 44–56, 2020.
- [18] K. Li, R. Bacher, S. Schmidt, W. Leemans, and F. Steinicke, "Reality fusion: Robust real-time immersive mobile robot teleoperation with volumetric visual data fusion," in *2024 IEEE/RSJ International Conference on Intelligent Robots and Systems (IROS)*. IEEE, 2024, pp. 8982–8989.
- [19] F. De Pace, G. Gorjup, H. Bai, A. Sanna, M. Liarokapis, and M. Billinghurst, "Leveraging enhanced virtual reality methods and environments for efficient, intuitive, and immersive teleoperation of robots," in *2021 IEEE International Conference on Robotics and Automation (ICRA)*. IEEE, 2021, pp. 12967–12973.
- [20] P. Stotko, S. Krumpen, M. Schwarz, C. Lenz, S. Behnke, R. Klein, and M. Weinmann, "A vr system for immersive teleoperation and live exploration with a mobile robot," in *2019 IEEE/RSJ International Conference on Intelligent Robots and Systems (IROS)*. IEEE, 2019, pp. 3630–3637.
- [21] F. Huang, X. Yang, T. Yan, and Z. Chen, "Telepresence augmentation for visual and haptic guided immersive teleoperation of industrial manipulator," *ISA transactions*, vol. 150, pp. 262–277, 2024.
- [22] S. Soroushpour and A. Shahdi, "Model predictive control for transparent teleoperation under communication time delay," *IEEE Transactions on Robotics*, vol. 22, no. 6, pp. 1131–1145, 2006.
- [23] N. Feizi, R. V. Patel, M. R. Kermani, and S. F. Atashzar, "Adaptive wave reconstruction through regulated-bmflc for transparency-enhanced telerobotics over delayed networks," *IEEE Transactions on Robotics*, vol. 38, no. 5, pp. 2928–2942, 2022.
- [24] D. A. Lawrence, "Stability and transparency in bilateral teleoperation," *IEEE transactions on robotics and automation*, vol. 9, no. 5, pp. 624–637, 1993.
- [25] K. Hashtroodi-Zaad and S. E. Salcudean, "Transparency in time-delayed systems and the effect of local force feedback for transparent teleoperation," *IEEE Transactions on Robotics and Automation*, vol. 18, no. 1, pp. 108–114, 2002.

[26] Z. Chen, F. Huang, W. Sun, J. Gu, and B. Yao, "Rbf-neural-network-based adaptive robust control for nonlinear bilateral teleoperation manipulators with uncertainty and time delay," *Ieee/Asme Transactions on Mechatronics*, vol. 25, no. 2, pp. 906–918, 2019.

[27] S. Guo, Z. Liu, J. Yu, P. Huang, and Z. Ma, "Adaptive practical fixed-time synchronization control for bilateral teleoperation system with prescribed performance," *IEEE Transactions on Circuits and Systems II: Express Briefs*, vol. 69, no. 3, pp. 1243–1247, 2021.

[28] Z. Chen, F. Huang, W. Chen, J. Zhang, W. Sun, J. Chen, J. Gu, and S. Zhu, "Rbfnn-based adaptive sliding mode control design for delayed nonlinear multilateral telerobotic system with cooperative manipulation," *IEEE Transactions on Industrial Informatics*, vol. 16, no. 2, pp. 1236–1247, 2019.

[29] Z. Chen, F. Huang, C. Yang, and B. Yao, "Adaptive fuzzy backstepping control for stable nonlinear bilateral teleoperation manipulators with enhanced transparency performance," *IEEE transactions on industrial electronics*, vol. 67, no. 1, pp. 746–756, 2019.

[30] F. Huang, X. Yang, D. Mei, and Z. Chen, "Unified contact model and hybrid motion/force control for teleoperated manipulation in unknown environments," *IEEE/ASME Transactions on Mechatronics*, 2024.

[31] T. Slama, A. Trevisani, D. Aubry, R. Oboe, and F. Kratz, "Experimental analysis of an internet-based bilateral teleoperation system with motion and force scaling using a model predictive controller," *IEEE Transactions on Industrial Electronics*, vol. 55, no. 9, pp. 3290–3299, 2008.

[32] F. Ferraguti, M. Bonfe, C. Fantuzzi, and C. Secchi, "Optimized power modulation in wave-based bilateral teleoperation," *IEEE/ASME Transactions on Mechatronics*, vol. 26, no. 1, pp. 276–287, 2020.

[33] M. Jorda, M. Vulliez, and O. Khatib, "Local autonomy-based haptic-robot interaction with dual-proxy model," *IEEE Transactions on Robotics*, vol. 38, no. 5, pp. 2943–2961, 2022.

[34] T. Kastritsi, T. P. Semetzidis, and Z. Doulgeri, "Passive bilateral surgical teleoperation with rcm and spatial constraints in the presence of time delays," *IEEE Transactions on Robotics*, 2024.

[35] S. Siroouspour, "Modeling and control of cooperative teleoperation systems," *IEEE Transactions on Robotics*, vol. 21, no. 6, pp. 1220–1225, 2005.

[36] D. Sun, Q. Liao, and A. Loutfi, "Single master bimanual teleoperation system with efficient regulation," *IEEE Transactions on Robotics*, vol. 36, no. 4, pp. 1022–1037, 2020.

[37] S. Tafazoli, S. E. Salcudean, K. Hashtroodi-Zaad, and P. D. Lawrence, "Impedance control of a teleoperated excavator," *IEEE Transactions on Control Systems Technology*, vol. 10, no. 3, pp. 355–367, 2002.

[38] V. Banthia, K. Zareinia, S. Balakrishnan, and N. Sepehri, "A lyapunov stable controller for bilateral haptic teleoperation of single-rod hydraulic actuators," *Journal of Dynamic Systems, Measurement, and Control*, vol. 139, no. 11, p. 111001, 2017.

[39] K. Zarei-nia, N. Sepehri, and Q. Wu, "A lyapunov controller for stable haptic manipulation of hydraulic actuators," *International Journal of Robust and Nonlinear Control*, vol. 22, no. 3, pp. 241–261, 2012.

[40] X. Liang, Z. Yao, W. Deng, and J. Yao, "Adaptive neural network finite-time tracking control for uncertain hydraulic manipulators," *IEEE/ASME Transactions on Mechatronics*, 2024.

[41] Z. Xu, W. Deng, H. Shen, and J. Yao, "Extended-state-observer-based adaptive prescribed performance control for hydraulic systems with full-state constraints," *IEEE/ASME Transactions on Mechatronics*, vol. 27, no. 6, pp. 5615–5625, 2022.

[42] J. Koivumäki, W.-H. Zhu, and J. Mattila, "Energy-efficient and high-precision control of hydraulic robots," *Control Engineering Practice*, vol. 85, pp. 176–193, 2019.

[43] J. Koivumäki and J. Mattila, "Stability-guaranteed impedance control of hydraulic robotic manipulators," *IEEE/ASME Transactions On Mechatronics*, vol. 22, no. 2, pp. 601–612, 2016.

[44] S. Lampinen, J. Koivumäki, W.-H. Zhu, and J. Mattila, "Force-sensorless bilateral teleoperation control of dissimilar master-slave system with arbitrary scaling," *IEEE Transactions on Control Systems Technology*, vol. 30, no. 3, pp. 1037–1051, 2021.

[45] S. Lampinen, J. Koivumäki, and J. Mattila, "Full-dynamics-based bilateral teleoperation of hydraulic robotic manipulators," in *2018 IEEE 14th International Conference on Automation Science and Engineering (CASE)*. IEEE, 2018, pp. 1343–1350.

[46] —, "Bilateral teleoperation of a hydraulic robotic manipulator in contact with physical and virtual constraints," in *Fluid Power Systems Technology*, vol. 51968. American Society of Mechanical Engineers, 2018, p. V001T01A021.

[47] S. Luo, M. Cheng, R. Ding, F. Wang, B. Xu, and B. Chen, "Human-robot shared control based on locally weighted intent prediction for a teleoperated hydraulic manipulator system," *IEEE/ASME Transactions on Mechatronics*, vol. 27, no. 6, pp. 4462–4474, 2022.

[48] R. Ding, M. Cheng, Z. Han, F. Wang, and B. Xu, "Human-machine interface for a master-slave hydraulic manipulator with vision enhancement and auditory feedback," *Automation in Construction*, vol. 136, p. 104145, 2022.

[49] P. Garrec, "Design of the arm exoskeleton able achieving torque control using ball screw and cable mechanism," in *Wearable Robotics*. Elsevier, 2020, pp. 45–66.

[50] T. Z. Zhao, V. Kumar, S. Levine, and C. Finn, "Learning fine-grained bimanual manipulation with low-cost hardware," *arXiv preprint arXiv:2304.13705*, 2023.

[51] M. Hejrati and J. Mattila, "Physical human–robot interaction control of an upper limb exoskeleton with a decentralized neuroadaptive control scheme," *IEEE Transactions on Control Systems Technology*, 2023.

[52] —, "Orchestrated robust controller for the precision control of heavy-duty hydraulic manipulators," *arXiv preprint arXiv:2312.06304*, 2023.

[53] —, "Decentralized nonlinear control of redundant upper limb exoskeleton with natural adaptation law," in *2022 IEEE-RAS 21st International Conference on Humanoid Robots (Humanoids)*. IEEE, 2022, pp. 269–276.

[54] K. P. Tee, S. S. Ge, and E. H. Tay, "Barrier lyapunov functions for the control of output-constrained nonlinear systems," *Automatica*, vol. 45, no. 4, pp. 918–927, 2009.

[55] M. Hejrati and J. Mattila, "Impact-resilient orchestrated robust controller for heavy-duty hydraulic manipulators," *arXiv preprint arXiv:2408.09147*, 2024.

[56] B. Hannaford, "A design framework for teleoperators with kinesthetic feedback," *IEEE transactions on Robotics and Automation*, vol. 5, no. 4, pp. 426–434, 1989.

[57] M. Gonzalez-Franco and T. C. Peck, "Avatar embodiment towards a standardized questionnaire," *Frontiers in Robotics and AI*, vol. 5, p. 74, 2018.

[58] W.-H. Zhu, *Virtual decomposition control: toward hyper degrees of freedom robots*. Springer Science & Business Media, 2010, vol. 60, section 3.3.5.